Journal of
Materials Chemistry A

Materials for energy and sustainability

Accepted Manuscript

This article can be cited before page numbers have been issued, to do this please use: B. Martínez-Sánchez, J. Quilez-Bermejo, E. San Fabián, D. Cazorla-Amorós and E. Morallon, *J. Mater. Chem. A*, 2022, DOI: 10.1039/D1TA10322A.

ROYAL SOCIETY OF CHEMISTRY

rsc.li/materials-a

On the mechanism of electrochemical functionalization of carbon nanotubes with different structures with aminophenylphosphonic acid isomers. An experimental and computational approach

Beatriz Martínez-Sánchez[a], Javier Quílez-Bermejo[b], Emilio San-Fabián[a], Diego Cazorla-Amorós[b], Emilia Morallón[a].

[a] *Departamento de Química Física and Instituto Universitario de Materiales de Alicante (IUMA), University of Alicante, Ap. 99, 03080, Alicante, Spain*

[b] *Departamento de Química Inorgánica and Instituto Universitario de Materiales de Alicante (IUMA), University of Alicante, Ap. 99, 03080, Alicante, Spain*

Abstract

Electrochemical functionalization of Single-Walled Carbon Nanotubes and Herringbone Carbon Nanotubes (SWCNTs and hCNTs, respectively) has been successfully performed with aminophenylphosphonic acid isomers by potentiodynamic treatment in oxidative conditions. Exceptional selectivity and control of the functional species embedded into the Carbon Nanotubes (CNTs) have been achieved by carefully optimizing the electrochemical conditions in the functionalization. X-ray photoelectron spectroscopy (XPS) analysis determined a maximum heteroatom incorporation of *ca*. 2.3-2.6 at. % N and 1.4-1.6 at. % P when 2-aminophenylphosphonic acid (2APPA) is used with both carbon materials, probably because of the linear polymeric growth comparable to that of oligomers derived from aniline (ANI). However, the polymeric product obtained with 4-aminophenylphosphonic acid (4APPA) is much more limited, giving rise to a branched structure. In addition, electrochemical characterization, Raman spectroscopy and electron microscopy suggest that SWCNTs structure facilitates the oligomerization of longer but less stable chains through π-π interactions with the walls of CNTs, while hCNTs promote a more stable attachment according to their heterogeneity and higher reactivity. Computational calculations have confirmed the experimental results obtained, which allow us to shed more light on the mechanisms of the electrochemical functionalization of CNT with phosphorus and nitrogen-containing polymers.

Keywords: carbon nanotubes; electrochemical functionalization; nitrogen; phosphorus

DOI: 10.1039/D1TA10322A

1. Introduction

Carbon materials have played a crucial role in the development of nanotechnology in many research fields of science and engineering over the last years. Among the wide variety of structures and intrinsic properties, carbon nanotubes (CNTs) arise as key materials due to their astonishing mechanical, physico-chemical and electronic properties, thermal stability, as well as large accessible surface area [1,2]. Different synthesis methods have been exploited for growing CNTs with different quality and morphology (*i.e.* Single- (SW), Double- (DW) or Multi-Walled (MW)) under controlled conditions [3–5]. Other morphologies can also be found, such as Bamboo or Herringbone type CNTs [6]. However, raw CNTs samples usually contain significant amount of impurities and by-products of synthesis process, including amorphous carbon and/or catalytic metal nanoparticles, which can affect considerably their applicability [1,7]. To fully exploit their outstanding properties, several physical and chemical purification processes have recently been reported, in which chemical ones highlight because of their effectiveness and higher purity achieved [8], either under mild [9,10] or harsh oxidizing routes [11,12]. Latter treatments can lead to remarkable structural and length changes in CNTs by introducing defects along the conjugated structure or oxygen-containing groups [11,13]. In fact, defect sites incorporated throughout acid treatments, such as five carbon rings and additional chemical functional groups, are known as highly reactive sites and preferential points for oxidation [8].

Functionalization of CNTs is one of the most widespread procedures to modify and modulate their reactivity, conductivity, stability and structure. First strategies of functionalization were carried out in order to break down their poor dispersibility, due to their tendency to self-assemble into bundles by van der Waals forces, driving towards more manageable multifunctional materials with tunable properties, thereby extending their applications [2,13–15]. Two main approaches have been widely developed for the chemical modification of CNTs [13]. On the one hand, non-covalent functionalization is based on the interactions generated between the π conjugation system of CNTs and the modifier agent which incorporates the functionalities [15,16]. These can take place by van der Waals forces, hydrogen bonds, π-stacking, electrostatic and other interactions [13,16], therefore the structural integrity of the pristine material is preserved. Recently, non-covalent modification of CNTs wrapped with surfactants and polymers have been

View Article Online
DOI: 10.1039/D1TA10322A

frequently employed [15–17]. Here it is worth mentioning polymers as one of the most promising functionalization agents since the nature, length and amount of such polymers can be adjusted to the desired properties. Nevertheless, the weak interaction between CNTs and the modifier molecule can lead to a lack of coating stability [18]. On the other hand, covalent functionalization consists of direct attachment of functional and organic moieties to CNTs tips or sidewalls through chemical reactions (*e.g.,* carboxylation, amidation, esterification, thiolation, halogenation, cycloadditions, electrophilic and nucleophilic or racial additions, etc.) [13,14,19]. Control over the nature and stability of the functionalities linked to the CNTs are some of its advantages. It could also be distinguished between direct and indirect covalent functionalization, the latter when functional species, such as carboxylic groups, are generated on CNTs surface prior to the incorporation of other functionalities [20,21]. Additionally, there are two different methodologies for the covalent attachment of polymers, which are known as "grafted to" and "grafted from", depending on whether it is the polymeric chain or the monomer that initially links to the nanotube [22]. Unfortunately, covalent strategy involves a change of carbon atom hybridization from sp^2 to sp^3 and an increase in structural defects, affecting the intrinsic conductivity and mechanical strength of the CNTs [13,14,20]. Therefore, new methodologies of functionalization have been focused on finding a compromise between both types of surface modification.

Diverse routes have been employed for the successful modification of CNTs, for example by chemical, electrochemical, photochemical or thermal processes. Although chemical functionalization of CNTs enables the incorporation of effective and stable functionalities, lack of control and a high amount of reagents, most of them organic solvents and toxics, make this procedure non-cost efficient also from the environmental point of view [23]. In this sense, electrochemical methods have been widely used as a well-suited tool for the tailorable design of functionalized CNTs with more precise control and selectivity over the composition and functional species, by carefully adjusting the electrochemical oxidative (anodic) or reductive (cathodic) coupling conditions. Furthermore, they are promising for their simplicity and low cost, even working at near room temperature and atmospheric pressure with small volumes, low amounts of reagents and mainly using aqueous solutions [24–26].

Owing to their potential applications, the combination of CNTs with conducting polymers, such as polypyrrole (PPy) and polyaniline (PANI), has experienced fast-

paced growth, leading to, for example, excellent PANI/carbon nanostructured composites. In this context, the use of CNTs coordinated with functional polyaniline-like polymers and its derivatives has focused on obtaining heteroatom-containing carbon-based nanomaterials with enhanced features for different applications, such as electrocatalysis or biosensing [27–30]. Particularly, recent advances have demonstrated that co-doping with nitrogen and phosphorus can remarkably enhance the electrocatalytic activity of carbon materials through synergistic effects [28,31]. Moreover, they can act as promising supports of precious and non-precious metal nanoparticles [2]. Hence, electrochemical synthesis methodologies are now intensively studied for the co- and multi-doping of nanostructured carbon materials.

Specifically, our research group has developed an intense experimental work on the electrochemical polymerization of aniline monomers *para*-substituted with different functional groups in its structure (sulfonic, phosphonic, carboxylic, etc.) and in the presence of CNTs [27,32–34]. Additionally, the incorporation of heteroatoms into CNTs has been also studied by using other chemical methods [35]. Nonetheless, the mechanism of functionalization has not been explored in detail from a fundamental and theoretical points of view so far. It is also known that the position of the substituents in the aromatic ring affects the interaction with the electrode support, as well as the polymeric properties [36–38]. Therefore, a systematic study of such effect would be convenient in many cases. In addition, many of the previous works have focused on the electrochemical functionalization of both Single-Walled Carbon Nanotubes (SWCNTs) [32] and Multi-Walled Carbon Nanotubes (MWCNTs) [27,33,34], but without further purification treatments. However, it has been demonstrated that the presence of trace metal residues from their synthesis or modification methods could lead to misleading results in specific applications [39]. It should be noted that SWCNTs and MWCNTs present certain similarities, but also striking differences that must be considered. On the one hand, MWCNTs have numerous advantages due to their cost-effective production on a larger scale [40], high electrochemical and thermal resistivity [2]. On the other hand, SWCNTs have also shown many other interesting properties that make them ideal for energy-related applications. For example, SWCNTs have proven better electrical properties, together with higher tensile strength, flexibility and thermal conductivity compared to MWCNTs [2,41]. Specifically, oxidized SW/DWCNTs have demonstrated higher reactivities and activities towards the oxygen reduction reaction than MWCNTs,

View Article Online
DOI: 10.1039/D1TA10322A

which was largely attributed to the curvature of smaller diameters [42]. The presence of DWCNTs is of great interest for their selective functionalization of their outer wall, with higher thermal stability and mechanical strength than pure SWCNTs, while preserving their potential properties of the non-damaged inner-tube [43]. To the best of our knowledge, the electrochemical functionalization of other structures of CNTs, such as Herringbone-type CNTs (hCNTs), has not been studied in-depth for this purpose and compared in the literature, even though they are cheaper and their structure can be beneficial due to their large number of highly reactive sites (e.g., defects, edges, etc.). Actually, a previous work published by our research group [29] demonstrated promising results by using functionalized hCNTs for sensor applications, although further study is still required.

To understand the mechanism of the electrochemical modification of CNTs with organic aromatic molecules, it is important to predict their intermolecular adsorption process on the surface of CNTs, as well as the chemical structures expected when two or more aromatic species interact. Here, quantum chemical computational methods have been increasingly used [44]. In this respect, many theoretical studies have focused on non-covalent interactions between various molecules and the walls of SWCNTs [45,46], although other probable interactions with edges, defects and other configurations of CNTs should not be ruled out. However, to the best of our knowledge, the mechanisms of the electrochemical functionalization of different CNTs with phosphorus and nitrogen-containing polymers are still unclear.

In the present work, we have faced this challenging target through a versatile approach, including well-controlled electrochemical functionalization of CNTs with different structural arrangement, including SWCNTs and hCNTs, in the presence of phosphorus and nitrogen-containing monomers, aminophenylphosphonic acid isomers (2APPA or 4APPA). Exceptional control of surface modification of CNTs with N and P heteroatoms has been achieved by carefully selecting the potential in the electrochemical oxidation process. The effect of the structure of CNTs and the position of the phosphonic group in the APPA monomer is analyzed in detail, showing remarkable differences in the stability and the degree of N and P incorporation. In order to deepen into the mechanism, the experimental results are supported by computational calculations, what allow us to get a theoretical view based on first-principles

View Article Online
DOI: 10.1039/D1TA10322A

calculations and to shed light on important factors about the mechanism of functionalization.

2. Experimental

2.1. Reagents

Single-Walled/Double-Walled Carbon Nanotubes (SW/DWCNTs) with 99% of purity (outer diameter: 1-4 nm, length: 3-30 μm) and a specific surface area of around 587 m^2 g^{-1}, obtained by nitrogen isotherm at 77 K using the Brunauer Emmett and Teller (BET) method, were supplied by Cheap Tubes Inc. (Brattleboro, Vt, USA). Herringbone Carbon Nanotubes (hCNTs) were purchased from Tokyo Chemical Industry with 95% of purity (outer diameter: 10-20 nm, length: 5-15 μm) and a specific surface area of 123 m^2 g^{-1} [42]. Nevertheless, SWCNTs have certain amount of residual metallic impurities from the catalyst used for their synthesis, so they were subjected to a purification treatment described below. hCNTs do not reveal any surface metal content and they were used without further purification.

The *ortho*- and *para*- aminophenylphosphonic acids (2APPA and 4APPA, respectively, ≥95%) were supplied by Chem Space (Riga, Lithuania). Aniline (ANI) ACS reagent (≥99.5%) was obtained from Sigma-Aldrich. Distillation of ANI in vacuum was carried out in order to remove oligomeric products generated during storage. It was stored in the refrigerator (about 4ºC) before use. 4-Aminodiphenylamine (4ADPA), benzidine (BZ) and phenazine (PhzR) were also provided by Sigma-Aldrich. Sulphuric acid (H_2SO_4, 98%), potassium hydroxide (KOH, 85%) and dipotassium hydrogen phosphate tri-hydrate ($K_2HPO_4 \cdot 3H_2O$) were purchased from VWR Chemicals. Potassium dihydrogen phosphate (K_2HPO_4) were supplied by Merck. N, N-dimethylformamide (DMF), extra pure, employed as dispersant of CNT, was provided by Scharlau. Hydrochloric acid (HCl, 37%) and nitric acid (HNO_3, 69%) used as purifying and oxidizing agent of SWCNT, respectively, were purchased from PanReac AppliChem (ITW Reagents). All aqueous solutions were prepared with ultrapure water (18.2 MΩ·cm, Millipore® Milli-Q® water). Nitrogen gas (N_2, 99.999%) was supplied by Carburos Metálicos.

2.2. Purification treatment of Single-Walled Carbon Nanotubes

View Article Online
DOI: 10.1039/D1TA10322A

The removal of the residual metallic impurities was achieved by subjecting the pristine SWCNTs to a mild oxidative treatment with a mixture of nitric acid and hydrochloric acid (HNO_3:HCl = 3:5, molar ratio), in order to open the tube caps and allow higher accessibility to their entire surface. Consequently, it is possible to incorporate surface oxygen groups at defective sites by chemical oxidation, but without damaging their distinctive properties and structure. For this purpose, 200 mg of pristine SWCNTs were introduced into a two-necked balloon flask along with 100 mL of the acid mixture at 70ºC for 12 h under reflux conditions (a-SWCNTs). Additionally, a similar purification treatment was performed only in the presence of 5 M HCl at 50ºC overnight (b-SWCNTs) by following the purification treatment described in the literature [42], for comparison purposes. Afterwards, the samples were filtered and washed several times with deionized water until a pH value of about 7 was reached. They were finally dried in an oven at 120ºC in air overnight, resulting in a-SWCNTs and b-SWCNTs samples, respectively.

2.3. Electrochemical functionalization of CNTs with 2APPA and 4APPA

2.3.1. Electrode preparation

The working electrode (WE) for electrochemical modification was prepared by dropping a 1 mg mL^{-1} dispersion of each type of CNTs in DMF. The dispersion was previously homogenized via ultrasonication for at least 40 min. Glassy carbon electrode surface (GC, 3 mm diameter), employed as the WE, was carefully sanded with fine emery paper and polished with alumina slurries, following by a rinse with ultrapure water. Then, two aliquots of 5 μL of the CNTs dispersion were casted onto GC surface and dried using an infrared heating lamp to evaporate the solvent. The procedure was repeated twice to attain an electrode loading of 0.14 mg cm^{-2}. Prior to their use, modified GC electrode is immersed in the study solution for *ca.* 1 h for the entire porosity to be accessible to the working electrolyte.

2.3.2. Modification of CNTs with nitrogen and phosphorus functional species

Electrochemical modification of CNTs was performed using a BioLogic SP300 Potentiostat-Galvanostat. The electrochemical set-up was a standard three-electrode cell, where the GC modified with the CNTs was the working electrode (WE), a graphite rod was used as the counter electrode (CE) and a Ag/AgCl/Cl^-(sat) electrode connected with the electrolyte in a Luggin capillary as the reference electrode (RE). However, all

View Article Online
DOI: 10.1039/D1TA10322A

the potentials in this work are referred to the reversible hydrogen electrode (RHE). The WE was immersed at a controlled potential of 0.2 V to avoid the initial oxidation of monomers. Subsequently, electrochemical functionalization of CNTs was achieved by submitting the sample to a cyclic voltammetry (CV) during 10 cycles at 10 mV s^{-1}, in an aqueous electrolyte of 0.5 M H_2SO_4 containing 1 mM 2APPA or 1 mM 4APPA at room temperature. In all cases, the working solutions were deoxygenated by bubbling N_2 during 20 min before starting the experiments and this atmosphere was maintained during the experiments. Upper potential limit was varied in order to analyze its influence in the functionalization. After electrochemical modification, the WE was repeatedly washed with ultrapure water to remove the remaining electrolyte.

2.4. Electrochemical characterization

Electrochemical behaviour of the functionalized CNTs electrodes was performed using the same electrochemical three-electrode system configuration as those referred in the previous section, but free of monomer. Three deoxygenated aqueous solutions with different pH were employed as electrolytes: acid (0.5 M H_2SO_4), neutral (0.1 M PBS, pH=7.2) and alkaline medium (0.1 M KOH). All the characterization was performed in a potential range from 0 V to 1.0 V at 50 mV s^{-1}.

2.5. Physico-chemical characterization

Compositional and chemical analysis were performed by X-ray photoelectron spectroscopy (XPS) with a VG-Microtech Multilab 3000 spectrometer equipped with a semispherical electron analyzer with 9 channeltrons (passing energy of 2-200 eV) and an X-ray source with Al radiation (Kα 1253.6 eV). The deconvolutions of the P2p and N1s peaks were done by minimum squares fitting using Gaussian-Lorentzian curves, while the Shirley method was used for background determination. The P2p spectra were analyzed considering the spin-orbit splitting into $P2p_{3/2}$ and $P2p_{1/2}$ with a 2:1 peak area ratio and 0.87 eV splitting.

Raman spectra were collected by a Jasco NRS-5100 spectrometer, using a 532 nm solid-state laser (green) at 3.9 mW, a 20x objective (MPLFLN) and a focal distance of 300 mm. Calibration of the spectrometer was performed with a Si slice (521±2 cm^{-1}) in order to check the response peak at 520 cm^{-1} and to eliminate possible interferences by the effect of fluorescence. Each spectrum was collected after 120 s.

View Article Online
DOI: 10.1039/D1TA10322A

Temperature programmed desorption (TPD) experiments provide information about the nature and amount of surface functional groups of carbon material. TPD measurements were performed in a DSC-TGA system (TA Instruments, SDT Q600 Simultaneous) coupled to a mass spectrometer (HiCube 80 Eco, Pfeiffer Vacuum, Germany). The samples were heat treated up to 900ºC (heating rate 10ºC min^{-1}), after an intermediate drying step at 120ºC, under a helium flow rate of 100 mL min^{-1}. Amounts of CO and CO_2 desorbed from the sample, among other relevant signals, were monitored and quantified by a previous calibration using calcium oxalate. Nature and quantity of different carbon-oxygen groups depend on the starting material and treatments. CO_2 desorption mainly occurs from decomposition of carboxylic acids, anhydrides and lactones, whereas CO desorption mainly comes from decomposition of anhydrides, phenol, carbonyl/quinone and ether groups [47].

Microstructural characterization of the different materials was performed by transmission electron microscopy (TEM). In this study, TEM images were taken with a JEOL JEM-2010 model, INCA Energy TEM 100 model microscope with an electron beam of 200 keV, equipped with a GATAN acquisition camera. Regarding sample preparation, DMF was used to obtain a homogeneous suspension of CNTs which was dropped onto a copper grid and left to dry in air before the measurements.

2.6. Density functional theory calculations (DFT)

Computational chemistry [48] is a very useful tool that makes use of mathematical models to simulate interactions between atoms and thus to explain experimentally observed results. Moreover, theoretical calculations provide us with new insights and knowledge with predictive values. In this work, Density Functional Theory (DFT) calculations at B3LYP/6-31G(d) level [49–52] were utilized through Gaussian 09 software package [53]. Dispersive forces were considered and computed by using Grimme D3 scheme method [54] without solvent effect. Restricted and unrestricted solutions were considered for closed and open-shell systems, respectively. This level has proven to be accurate to simulate intermolecular weak interactions between aromatic molecules and CNTs [44].

The optimization of the geometry and the minimum energies were calculated neglecting vibrational corrections and the energies are reported in kJ mol^{-1}. The polymerization energies were calculated as the differences between the final products

View Article Online
DOI: 10.1039/D1TA10322A

and individual monomers energy. The model structure used for carbon nanotubes consists of armchair ended SWCNT tubes of 160 atoms and a diameter of 0.7 nm. This model has been used to reduce computational costs, considering that SWCNTs typically have a diameter between 1 – 2 nm. The adsorption energies of the CNTs and the monomers (ANI, 2APPA and 4APPA) were computed through the differences between the energies of the optimized structures of products and reagents. Adsorption energies were calculated as the differences in energy of each optimized geometry, neglecting vibrational corrections.

3. Results and discussion

3.1. Physico-chemical and morphological characterization of CNTs

TPD experiments were employed to confirm the effectiveness of the purification treatment on metal catalyst removal and to obtain an accurate knowledge of the surface chemistry. Figure S1 depicts the CO and CO_2 evolution profiles for pristine SWCNTs and after acid treatments. In all the cases, the CO evolution is higher than the CO_2 one. The sharp peak above 850ºC in the pristine SWCNTs is related with the metallic impurities. These metallic species can be partially oxidized in the pristine material and become reduced by the carbon material upon the heat treatment. This peak disappears in the a-SWCNTs and the metal is not detected by XPS (Table S1), showing that it is an efficient purification treatment. Interestingly, although Fe is detected by XPS after the treatment with only HCl (b-SWCNTs), TPD profile does not show any evidence for its presence. It seems that HCl treatment is appropriate for the dissolution of the exposed Fe species, remaining the metallic species located under the closed tube caps. Thus, this method is not useful to remove completely this metallic impurity. Figure S1 and Table S1, as well as the full XPS survey spectra in Figure S2, also verify that hCNTs do not require further purification.

Table S2 shows the total amounts of CO and CO_2 released during the experiments for each sample. The total oxygen content is estimated from the amount of CO + 2 CO_2 (μmol g^{-1}). It is clearly observed that CO and CO_2 desorption from the a-SWCNTs sample is higher than for b-SWCNTs, due to the oxidation achieved with the acid mixture compared to the treatment with only HCl (i.e., low oxidizing character). These oxygen functional groups can be used directly as anchoring sites or (electro)chemically

View Article Online
DOI: 10.1039/D1TA10322A

modified for a specific purpose. Owing to the chemical stability of carbon nanotubes, it could be assumed that oxygen groups are mostly located at CNTs edges and at defect sites. Profiles of hCNTs reveal a higher presence of oxygen compared to b-SWCNTs, due to the high density of edges (reactive sites) which are more easily oxidized [30].

Transmission electron microscopy (TEM) images are displayed in Figure 1, in which important morphological differences can be appreciated between the different types of CNTs. Figures 1A and B show the a-SWCNT and b-SWCNT samples as the regular tubular structure of carbon nanotubes with the single/double layer parallel to the axis of the nanotube. Nevertheless, a-SWCNTs reveal that treatment with the acid mixture promotes the presence of some defects and amorphous carbon residues along the walls, but without significative damage to the structure. It has been reported that carboxylated carbonaceous fragments (CCFs) appear covering the nanotubes as a byproduct of oxidative treatments [21]. Herringbone nanotubes, in Figure 1C, display a very different structure in which the conical graphite sheets are stacked providing a high concentration of graphitic edges. Furthermore, it is noteworthy that hCNTs have much more heterogeneous structure with a larger amount of surface defects than the other samples.

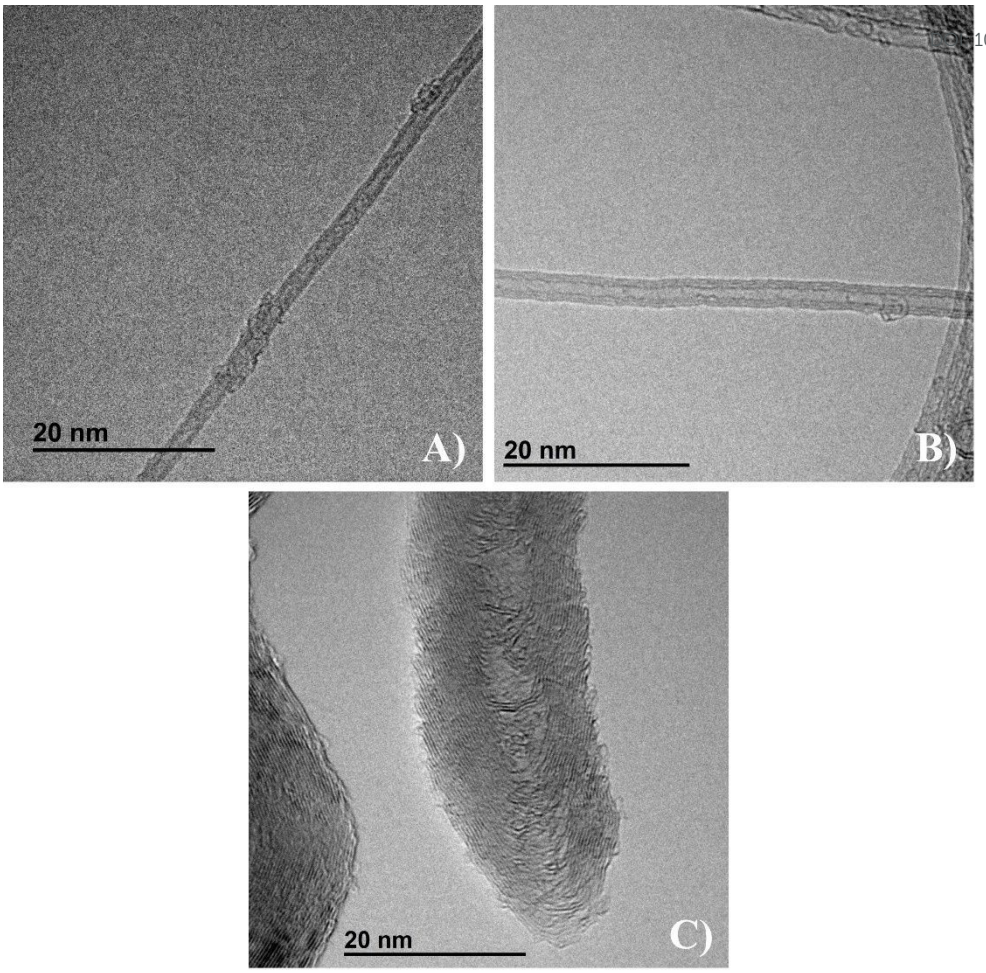

Figure 1. TEM images of A) a-SWCNT, B) b-SWCNT and C) hCNT.

Raman spectra (Figure S3) were acquired to obtain further information on the structural and physico-chemical properties of CNTs samples. In Figure S3A, the primary G band appears as the most important contribution at around 1570-1590 cm^{-1}. It originates from tangential modes associated with strain or stretching of the C-C bond in the plane [55,56]. The intensity and the position of the G band slightly changes with the acid treatments as a result of minor modifications in the electronic structure. As expected, G band in hCNTs sample shows more significant changes. The D band appears at around 1350 cm^{-1} and is often referred as the defect/disorder induced band [57,58], which is also associated with the presence of disordered amorphous carbon [59]. In the case of SWCNTs, it becomes slightly more intense after the oxidative treatment (a-SWCNT) due to the formation of some sp^3 carbon atoms defects on the surface of the carbon nanotube, where oxygen groups can be covalently attached. In the case of a-SWCNT, a shoulder on the low frequency side of the G band appears at

around 1560 cm^{-1}, which could correspond to the D** (or D'') mode [46]. This broad band could be assigned to interstitial disorders related to functionalization [79]. Nevertheless, this oxidative treatment produces small structural changes and incorporated oxygen-containing groups could be useful for many electrochemical properties and applications [60,61]. Another band related to the second order mode can be also appreciated at 2700 cm^{-1}, which is referred to as the G' or 2D band [55–57]. Consequently, the D and G' bands are highlighted for hCNTs, due to the higher defect density and heterogeneity in this material.

Radial Breathing Mode or RBM bands appear at the low frequency end of the spectra (100-350 nm) and correspond to vibration of the carbon atoms in the radial direction (Figure S3B). They are characteristic for SWCNTs and are sensitive to the nanotube diameter. Hence, a diameter distribution of 1.1-3.0 nm has been estimated by applying the general equation found in the literature [62], which has been corroborated by TEM images. Even though some RBM bands seem weaker after acid treatments, it can be assumed that the mean diameter in all the SWCNT samples remains almost unchanged.

3.2. Electrochemical behaviour of CNTs in acidic medium

Prior to the functionalization, electrochemical behaviour of a-SWCNTs, b-SWCNTs and hCNTs was tested. Figure S4 shows cyclic voltammograms obtained in an acidic aqueous solution (0.5 M H_2SO_4) during the stepwise opening of the upper potential limit from 0.80 to 1.8 V.

Cyclic voltammograms of a-SWCNT (Figure S4A) display the typical rectangular shape between 0.0 and 1.0 V but with the presence of a wide and reversible oxidation/reduction process that appears at around 0.50-0.60 V, which is related to the redox processes associated to the surface oxygen groups in carbon materials (*e.g.* hydroquinone/benzoquinone or anhydride groups) [63] as a consequence of the oxidative acid treatment [64]. Cyclic voltammograms for b-SWCNTs (Figure S4B) also show a rectangular shape without the appearance of any redox processes at lower oxidation potentials due to the milder purification treatment. As it is well-known, the main contribution to the cyclic voltammogram in carbon materials is the charge and discharge of the electric double-layer in which the double-layer capacitance can be correlated with the exposed CNTs surface available for its functionalization. Table S1 shows the gravimetric capacitance for all samples and it can be observed an increase in

View Article Online
DOI: 10.1039/D1TA10322A

the value for a-SWCNTs. This rise in the electrochemical accessible area can be largely related to the opening of the tips and the formation of some specific defects that facilitate the accessibility of the electrolyte towards the internal surface of the nanotubes, which is of great interest for their subsequent functionalization. Further increase in the upper potential limit above 1.1-1.2 V (Figure S4A and B), generates an intense oxidation current for the acid treated samples which is higher than the observed for the unpurified SWCNTs (Figure S5).

Regarding hCNTs (Figure S4C), the electrochemical response is quite different due to the distinct arrangement of the graphene sheets in their structure, in which the lower surface area results in a smaller gravimetric capacitance (Table S1). Nevertheless, the high density of edge sites results in a higher reactivity, as can be perceived in the oxidation current of each first cycle after increasing the anodic potential of the upper limit, with respect to the basal positions towards electron transfer processes [65].

So far, in-depth physico-chemical and electrochemical characterization performed for all the CNTs indicates that the oxidative purification treatment with HCl and HNO_3 (a-SWCNT) is the most effective for the removal of the residual metal catalyst. Furthermore, interesting surface oxygen functionalities are developed, but without significant damage of their structure. In contrast, the treatment with HCl (b-SWCNT) removes only part of the most accessible metal but leaves some traces in the nanotubes. Finally, hCNT has strong structural and reactivity differences compared to SWCNT. Therefore, a-SWCNTs and hCNT have been chosen for their electrochemical functionalization. Comparative results of the electrochemical modification of the b-SWCNTs are also shown in the Supporting Information.

3.3. Electrochemical functionalization of CNTs in presence of aniline in acidic medium

Owing to the extensive knowledge about the behaviour and properties of polyaniline, the electrochemical functionalization is first carried out in presence of aniline in the electrolyte (0.5 M H_2SO_4 + 1 mM ANI) for comparison purposes. Cycling scanning has been employed to assess the effect of the upper potential limit on CNTs functionalization (Figure 2). The appearance of new redox processes is observed by the presence of aniline, which is also affected by the structure of CNTs and their surface chemistry.

View Article Online
DOI: 10.1039/D1TA10322A

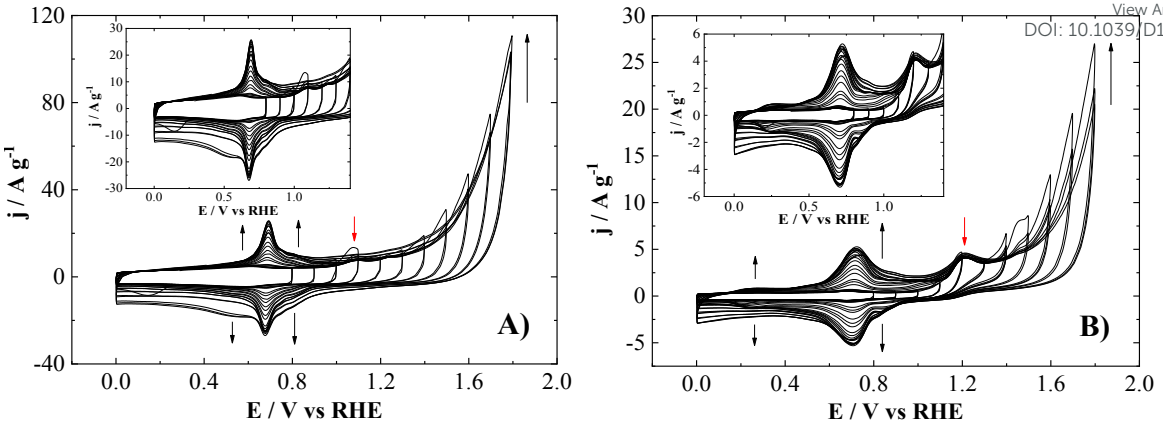

Figure 2. Cyclic voltammograms of the open stepwise upper potential limit from 0.80 to 1.8 V for A) a-SWCNT and B) hCNT, in 0.5 M H_2SO_4 + 1 mM ANI at 50 mV s^{-1}.

Figure 2 reveals that electrochemical response at low upper potential limits are quite similar to those observed in absence of the monomer (Figure S4). As the potential window is opened for a-SWCNTs (Figure 2A), an irreversible anodic peak appears at around 1.1 V (marked with a red arrow) corresponding to monomer oxidation, which decreases and slightly shifts to more positive potentials in the subsequent cycles. Interestingly, the structure and heterogeneity of hCNTs influence significatively the interaction with monomers and the monomer oxidation potential is shifted 0.1 V towards higher potentials (Figure 2B). This anodic peak, observed for both a-SWCNTs and hCNTs, can be associated with the one-electron oxidation of the amine group to the corresponding radical cation, which can act both as an initiator of polymerization through follow-up chemical reactions [66], as well as promoting the covalent coupling of C-N species to the CNTs surface [67,68].

Further polarization above the oxidation potential of monomers generates several redox processes at around 0.67V, as a result of the formation of different dimers, oligomers, radicals and other electroactive species over the CNTs surface. The increase in the current density with cycling of this redox processes is related to the growth of the oligomeric species or short-chain polymeric materials, which could interact by either covalent attachments or non-covalent physical adsorption through the π-electron structure of the nanotube sidewalls. Particularly, hCNTs give rise to wider and overlapped peaks, possibly due to the heterogeneity of the sites where aniline might interact.

Based on the previous results, different selected upper potential limits (1.0, 1.2, 1.4, 1.6 and 1.8 V) have been proposed for the electrochemical surface functionalization of CNTs by direct oxidation. Figure S6 shows the cyclic voltammograms at 1.2 and 1.4 V, in absence (black lines) and in presence of 1 mM ANI (colored lines) in acid aqueous solution (0.5 M H_2SO_4), during 10 cycles at 10 mV s^{-1}. High oxidation potentials lead to defects and film degradation due to the over-oxidation of the polymer structure. In the initial scan, an anodic peak related to the aniline oxidation is observed when cycling above 1.0 V. After the first cycle, different redox processes appear in the cyclic voltammograms, depending on the structure and the surface chemistry of the CNTs. The nature of these peaks will be discussed anon.

3.3.1. Electrochemical characterization of N-functionalized CNTs

Once the CNTs have been electrochemically modified with ANI and washed abundantly with ultrapure water, the electrochemical behaviour, stability and electroactivity of the materials were assessed in a three-electrode cell free of monomer at different pH. Here, three aqueous solutions were employed as electrolytes: acid medium (0.5 M H_2SO_4), neutral medium (0.1 M PBS, pH=7.2) and alkaline medium (0.1 M KOH).

Figures S7 and S8 shows the cyclic voltammograms recorded from 0.0 to 1.0 V for CNTs electrodes electrochemically modified at 1.0, 1.2, 1.4, 1.6 and 1.8 V, at different pH electrolytes. The presence of several redox peaks confirms the formation of electroactive species with N-containing moieties on the CNTs surface at all the studied potentials and electrolytes. Moreover, it has been proven that the main processes are related to surface species, since there is a linear fitting of the oxidations/reduction current with the scan rate in acid medium (Figure S9). Moreover, a-SWCNTs show higher voltametric charge compared with b-SWCNT modified with ANI (Figure S10), probably because of their higher accessible surface area and improved interactions with monomers by surface oxygen groups and defects. Since the tips of the a-SWCNTs can be opened through the oxidizing treatment, the channels of the carbon nanotubes may also act as nano-reactors where the probability of adsorption and reaction of molecules is higher than outside. Both, interactions between the amino groups and the surface oxygen groups and the dispersive π-π interactions between the delocalized π-electrons in the chemical structure of organic molecules and the graphene layers (walls of the carbon nanotubes), could be the main adsorption mechanisms [60,69]. On the other

View Article Online
DOI: 10.1039/D1TA10322A

hand, the voltametric charge of modified hCNTs is also lower, which suggests that polymeric growth is less favored. This effect could be related to the impediment of the correct π-π adsorption of oligomeric species on the surface, thus mainly promoting covalent binding of ANI molecules at high reactivity sites (defects and edge sites).

It is well-known that PANI growth preferentially takes place through the incorporation of monomers in *para*- position to the amino group (head-to-tail radical coupling) [66]. However, the monomer concentration in the electrolyte plays a critical role on the product distribution and, consequently, on the shape of cyclic voltammograms. High aniline concentrations results in two pairs of redox processes at around 0.40 V and 0.90 V related to the typical transition between polyaniline states, from leucoemeraldine to emeraldine (LE/EM) and from emeraldine to pernigraniline (EM/PN), respectively [70,71]. Nonetheless, relatively lower monomer concentrations could lead to a decrease of the monomer/radical-cation ratio and to the development of one or two wide "middle peaks", mainly assigned to dimers, degradation products related to oxidized PANI (benzoquinone/hydroquinone) [70] or crosslinked units [72].

Interestingly, Kuznetsov et al. [73] recently revealed that low monomer concentration results in the predominant development of low-weight intermediates at the early stages of aniline polymerization as final products. In this way, reversible peaks located at 0.60-0.70 V usually appear with lower aniline content and high potential, in agreement with the electrochemical behaviour observed in Figures S7 and S8. These redox processes could be attributed to either hydroquinone/benzoquinone transition [63], or products of aniline dimerization in acid medium (4-aminodiphenylamine, 4ADPA) [70,71]. Additionally, other wider and less intense peaks could appear at around 0.30 and 0.45 V. This is normally associated with the LE/EM transition [70,71,74], while others suggest the presence of phenazine-ring (PhzR) containing structures [75,76]. The presence of other polymeric products, such as benzidine (BZ), cannot be ruled out [71].

To deepen into these possibilities, the modification of a-SWCNTs with 4ADPA, BZ and PhzR at 1.2 V (vs RHE) has been analyzed (Figure S11). The observed redox processes have strong similarities with those observed after the modification of a-SWCNTs with aniline (Figure S7). Thus, most of the redox processes registered could be associated to the presence in the CNTs of a combination of similar related species together with oxygen functionalities, although there is some complexity in their interpretation because of the similarity of the voltammetric profiles. Therefore,

View Article Online
DOI: 10.1039/D1TA10322A

polyaniline-like intermediate units play an important role in defining the structure, morphology and properties of the final product.

Regarding the effect of the pH, a strong dependence on the electrochemical response and electroactivity is observed. Generally, as the pH is increased to a progressively more alkaline solution, a decrease in current density and a higher peak separation of the main redox processes are observed, especially at neutral medium. Nevertheless, when lower potentials (1.0 and 1.2 V) are used for CNTs modification, two overlapped, highly stable and reversible processes appear at around 0.55-0.70 V in alkaline solution (Figures S7 and S8). Since the main PANI-like redox processes are deactivated in alkaline electrolytes, the appearance of these basic-active pseudocapacitive components could be again attributed to 4ADPA related species (Figure S11A), thus confirming the previous hypothesis.

3.4. Electrochemical functionalization of CNTs with aminophenylphosphonic acid isomers in acidic medium

Following with the study, it is of great interest to evaluate the effect of incorporating phosphonic functional groups at different positions in the aniline aromatic ring. Preliminary studies are performed analogously to aniline (section 3.3.) in order to define the optimal conditions to functionalize the CNTs and this is explained in detail in the supporting information (Figure S12).

From these results, different upper potential limits were employed for the electrochemical surface functionalization of CNTs. Figures S13 and S14 show direct oxidation at 1.2 V and 1.4 V in absence (black lines) and in presence (colored lines) of 1 mM 2APPA and 1 mM 4APPA in acid aqueous solution, during 10 cycles at 10 mV s^{-1}, respectively.

The monomer incorporation in the growth of PANI-like polymer usually takes place in *para*- position to the amino group [66], when possible. However, some studies reveal that when *para*- position is occupied with functional groups, the growth process could proceed either through the *ortho*- or/and *meta*- positions [27,36], giving rise to short-chain oligomers with branched structure. Therefore, it is reasonable that in presence of 2APPA, the voltammetric profile shows similar electrochemical behaviour in comparison with the polymerization of ANI monomers under the same conditions since both polymers are expected to exhibit linear polymeric structures; whereas in presence

View Article Online
DOI: 10.1039/D1TA10322A

of 4APPA, the polymerization is expected to occur through *ortho-* or *meta-* positions, thus leading to a branched structure.

3.4.1. Electrochemical characterization of N and P-functionalized CNTs

Characterization of CNTs modified with N and P species have been carried out in a monomer-free acidic electrolyte. Figure 3 shows the steady voltammograms during the tenth cycle of a-SWCNTs and hCNTs functionalized with 2APPA (blue lines) and 4APPA (red lines) at 1.2 V (Figure 3A and C) and 1.4 V (Figure 3B and D). Electrochemical responses of unmodified CNTs (dashed lines), as well as those of CNTs modified with ANI (green lines) have also been displayed for comparison purposes.

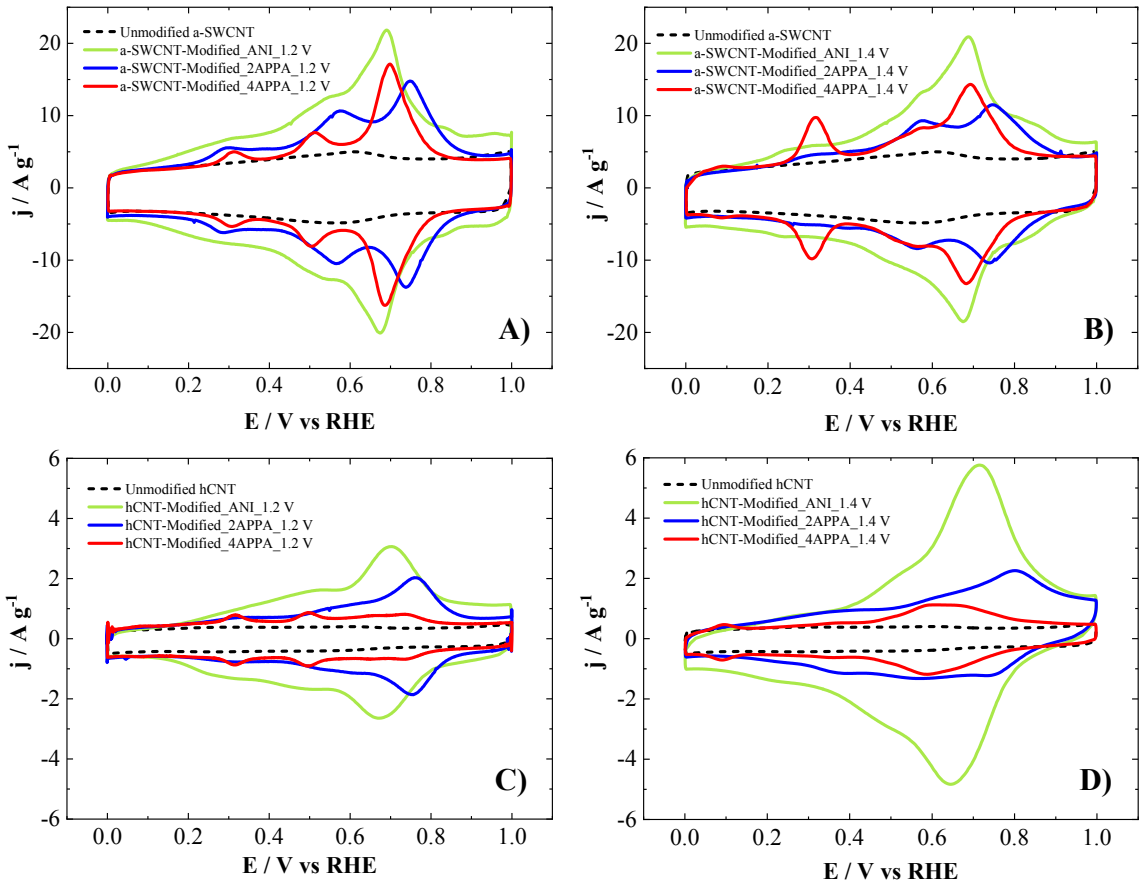

Figure 3. Cyclic voltammograms of A, B) a-SWCNT and C, D) hCNT unmodified (dashed lines) and electrochemically modified at A, C) 1.2 V and B, D) 1.4 V with 1 mM ANI (green lines), 1 mM 2APPA (blue lines) and 1 mM 4APPA (red lines), in acid medium (0.5 M H_2SO_4) free of monomers at 50 mV s^{-1}. 10^{th} cycle.

View Article Online
DOI: 10.1039/D1TA10322A

The development of electroactive species with N and P moieties onto CNTs surface is confirmed by the presence of several redox processes, different from the rectangular capacitive shape of non-electrochemically modified CNTs. The most straightforward effect of the incorporation of phosphonic groups onto CNTs surface is the appearance of new redox processes at low potentials, at around 0.10 and 0.31 V, when 4APPA is used, especially at higher oxidation potential (1.4 V) (Figure 3 B and D). The last process is also observed in presence of 2APPA and ANI, but with less intensity. Interestingly, these low potential redox processes seem to be related with PhzR-type structures (Figure S11C), which suggests that 4APPA promotes this sort of branched chains; while the more similar voltammetric profiles of 2APPA and ANI in Figure 3 suggest the development of more linear chains associated with 4ADPA (Figure S11A) dimers and other related oligomers and derivatives. When using 4APPA for the modification of a-SWCNTs, more defined and narrow processes than with 2APPA and ANI are observed. In addition, the redox processes at around 0.50-0.55 V and 0.70-0.75 V are shifted towards more positive potentials when 2APPA is used with respect to the other monomers, possibly induced by the electron-withdrawal effect of phosphonic groups from the polymer backbone.

Likewise, linear fitting of main redox processes with scan rate reveals that these are related to redox-active species at the electrode surface (Figures S15 and S16). Interestingly, the appearance of similar redox peaks was also reported for multiwall carbon nanotubes electrochemically functionalized with substituted amino-benzene acids [27]. Moreover, it is noticed again that a-SWCNT favor the interaction with monomers and development of these processes in terms of current density in comparison with b-SWCNTs (Figure S17), especially when ANI and 2APPA are used. It is worth noting that hCNTs modified with 4APPA show a lower response than with ANI and 2APPA, suggesting that 4APPA seems to be "deactivated" for the development of oligomeric species when interacts with the carbon atom edges in a higher extent than 2APPA and ANI. Therefore, the development and distribution of final monomeric/oligomeric products can be controlled by the chemical nature and structure of monomers and CNTs, as well as the electrochemical conditions used, among other factors [70].

Moreover, to shed more light on the nature of the electroactive polymeric species and their interaction to the carbon nanotubes, the a-SWCNTs and hCNTs modified with

View Article Online
DOI: 10.1039/D1TA10322A

APPA monomers at 1.2 V were subjected to a stability test in H_2SO_4 solution free of monomers by cyclic voltammetry during 150 cycles at 50 mV s^{-1} (Figure S18). Cyclic voltammograms clearly show the vanishing of some redox processes with successive cycling, mainly those that appear at 0.70-0.75 V and at 0.31 V (the last one only with 4APPA), whereas the peak at 0.50-0.55 V remains unchanged. This suggests the formation of different oligomeric materials, which interact predominantly by physical adsorption, together with some covalently attached species at the most reactive sites and probably related to monomers, dimers and short-chain species. Interestingly, hCNTs seem to promote more stable species, since the loss of signal of redox processes occurs to a lower degree than with the a-SWCNTs. Actually, XPS analysis after the stability test confirm these results (see next section).

The effect of electrochemical responses and electroactivity with the pH of the medium has also been studied. Figure S19 shows the cyclic voltammograms for CNTs electrochemically modified at 1.2 V, in monomer-free electrolytes with different pH. In general, an increase in irreversibility and a decrease in current density is promoted by increasing the pH of the solution. Consequently, only the process at around 0.70-0.75 V is slightly observed in alkaline medium, as in the case of modification with ANI (Figures S7 and S8).

Table S3 compares gravimetric capacitance before and after modification at 1.2 V and at different pH. Capacitances of CNTs submitted to the same polarization conditions in absence of monomers are also shown. The gravimetric capacitance values before and after modifying CNTs at 1.2 V in absence of monomer do not show significant changes, thus suggesting that the electrochemical oxidation under mild conditions does not affect the structure of CNTs. Therefore, it can be assumed that the contribution of the double-layer in the capacitance remains unchanged. In general, functionalized CNTs have higher capacitance compared to unmodified CNTs. Therefore, the improved capacitance values after electrochemical functionalization are mainly ascribed to pseudocapacitive contribution of redox processes due to organic electroactive species formed over CNTs surface. The best results of capacitance are achieved when ANI is used for the functionalization of CNTs, due to steric hindrances of voluminous chain-anchored phosphonic substituents. It is also noteworthy the influence of pH of the medium on the electroactivity of the species and, therefore, on the capacitance values. In this sense, the acid pH reveals the best responses in all cases.

View Article Online
DOI: 10.1039/D1TA10322A

However, the presence of surface redox species that can increase the capacitance in neutral and alkaline medium is very interesting for the further preparation of carbon materials.

The amount of functionalities introduced on the CNTs surface can be estimated from the differences in the electric charge determined in the voltammogram between the functionalized CNTs at 1.2 V in presence and in absence of monomers, taking into consideration that each redox process is associated to one electroactive species in which only one electron is transferred (Table S4). We have also assumed that all functionalities are electroactive in acid electrolyte.

3.4.2. Physico-chemical and morphological characterization of CNTs modified with N and P functional groups

XPS analysis were performed to gain more information about the chemical composition, the content of N and P species and the atomic environment of the functionalized CNTs. Table 1 shows the atomic percentages after the electrochemical incorporation of N and P functionalities on CNTs at different upper potential limits, together with those of unmodified CNTs for comparison purposes. Data for 1.0 V are not included since the low degree of modification produces inaccuracies in the measurement with values close to the detection limit of the XPS technique. An increase in oxygen content is observed with the upper potential limit, which can be related to both the phosphonic functionalities in oligomeric chains and the overall electrooxidation process of the oligomers and the CNTs. It can be observed that hCNTs suffer a higher oxidation degree under the same modification conditions, since they show higher oxygen increase at lower potential limits with respect to unmodified hCNTs. N/P atomic ratio sets the proportion of both functional groups, which should theoretically be 1:1. Table 1 reveals the release of some phosphonic groups, possibly due to the oxidizing conditions employed. Consequently, phosphonic groups are oxidized to phosphate or phosphoric species and subsequently hydrolyzed [32,77].

In all cases, the functionalization of different CNTs with 2APPA results in a higher degree of N and P heteroatoms in their atomic composition than with 4APPA, probably due to the impeded polymerization for *para*-substituted aminobenzenes [78]. Therefore, a maximum atomic content of around 2.3-2.6 % N and 1.4-1.6 % P is obtained, which also depends on the carbon nanotube structure, surface chemistry and the applied

View Article Online
DOI: 10.1039/D1TA10322A

potential (the optimum is found between 1.2 and 1.4 V). As can be observed in Table 1, hCNTs modified with 2APPA and 4APPA show a higher content of these heteroatoms, despite the lower development of polymeric chains, where the attachment of monomers and short-chain species seems to be favored in a larger extent through the highly reactive edge and defect sites forming more stable species. Table 1 also shows the XPS analysis after the stability test by cyclic voltammetry during 150 cycles (Figure S18), which confirms that species incorporated on hCNTs are electrochemically more stable, especially those obtained by using 2APPA. In the other cases, it seems that atomic content of P decreases in a higher degree than N heteroatoms, thus increasing the N/P ratio.

In addition, Table S5 shows an estimation of the molar percentages from active species determined by CV in Table S4 for 2APPA and 4APPA. When comparing the values in Table S5 with those of Table 1 at the same conditions (1.2 V), it can be observed that for the a-SWCNTs, they are around half, thereby it follows that a high proportion of the functionalities incorporated are electrochemically active. Nevertheless, the molar percentages in Table S5 for the hCNTs are quite lower than the atomic ones obtained by XPS. This effect corroborates that the anchoring of monomers or shorter oligomeric chains on hCNTs gives rise to different structures of functionalities with respect to the polymeric chains expected on a-SWCNTs, with a predominance of covalent attachment, thus changing their redox properties and resulting in a decrease in the electron transfer as observed in cyclic voltammograms (Figure 3C and D).

Table 1. Atomic composition obtained from the XPS spectra of a-SWCNT and hCNT electrochemically modified with 2APPA and 4APPA at different applied potentials. Percentages are referred to the respective atomic total.

Sample	Monomer	Potential / V vs RHE	O / at. %	N / at. %	P / at. %	N / P*
a-SWCNT	Unmodified		6.38	0.44	-	-
	2APPA	1.2	14.80	2.34	1.62	1.2
		*1.2***	*12.93*	*1.73*	*0.66*	*2.0*
		1.4	16.07	1.44	1.12	0.9
		1.6	17.56	1.40	0.59	1.6
		1.8	27.55	1.23	0.45	1.8
	4APPA	1.2	8.45	1.03	0.51	1.2

		*1.2***	*6.22*	*0.82*	*0.20*	*1.9*
		1.4	13.76	0.96	0.57	0.9
		1.6	15.28	1.16	0.68	1.1
		1.8	22.31	1.36	0.54	1.7
hCNT	Unmodified		3.71	-	-	-
	2APPA	1.2	13.70	1.65	0.84	2.0
		*1.2***	*11.67*	*1.59*	*0.81*	*2.0*
		1.4	17.89	2.58	1.35	1.9
		1.6	20.55	2.42	1.18	2.1
		1.8	12.46	1.48	0.52	2.8
	4APPA	1.2	7.22	1.26	0.57	2.2
		*1.2***	*6.31*	*1.10*	*0.40*	*2.8*
		1.4	11.54	1.96	0.79	2.5
		1.6	15.74	2.01	0.54	3.7
		1.8	17.13	2.04	0.41	5.0

* The N content of unmodified CNT has been subtracted for the calculation

** Measurements obtained after the stability test by cyclic voltammetry during 150 cycles in 0.5 M H_2SO_4

Different species could be figured out from the deconvoluted N1s and P2p spectra (Figure 4 and Figure 5, respectively) for the different CNTs functionalized at 1.2 and 1.4 V with both APPA monomers. Additionally, XPS full survey spectra are shown in Figure S20. The N1s core-level spectra were fitted with two main contributions related to distinct nitrogen species. The first peak observed at lower binding energies, at around 400.0 eV, can be assigned to neutral amine species (-NH-) [34] and commonly found in PANI-like structures [79,80]. Additionally, this peak can also have some contribution from amide groups (–C(=O)NH–) formed from condensation reactions between amino groups of monomers and oxygen groups in CNTs, thus producing covalent grafting [81,82]. The second contribution at higher binding energies (401.8 eV) is attributed to oxidized and positively charged N-species (N^+), such as radical cation (–$N^{\bullet+}$–) or protonated nitrogen (–NH_2^+–,–N^+H=) [83]. Moreover, an increase in the amount of N^+ species with the potential is observed. This contribution can be related to strong interactions between the amino groups and the surface oxygen groups or surface defects, as well as to the charge stabilization or the doping efficiency of oligomeric materials [84]. It is also possible that some contribution to the oxidized N-species comes from the oxidizing pre-treatment with nitric acid, thereby leading to N-O species.

View Article Online
DOI: 10.1039/D1TA10322A

Some differences in the environment surrounding the nitrogen atoms are appreciated in hCNTs, with a higher contribution of N^+ species, probably as a consequence of stronger interactions and covalent attachments of the monomers and the reactive edge sites [30].

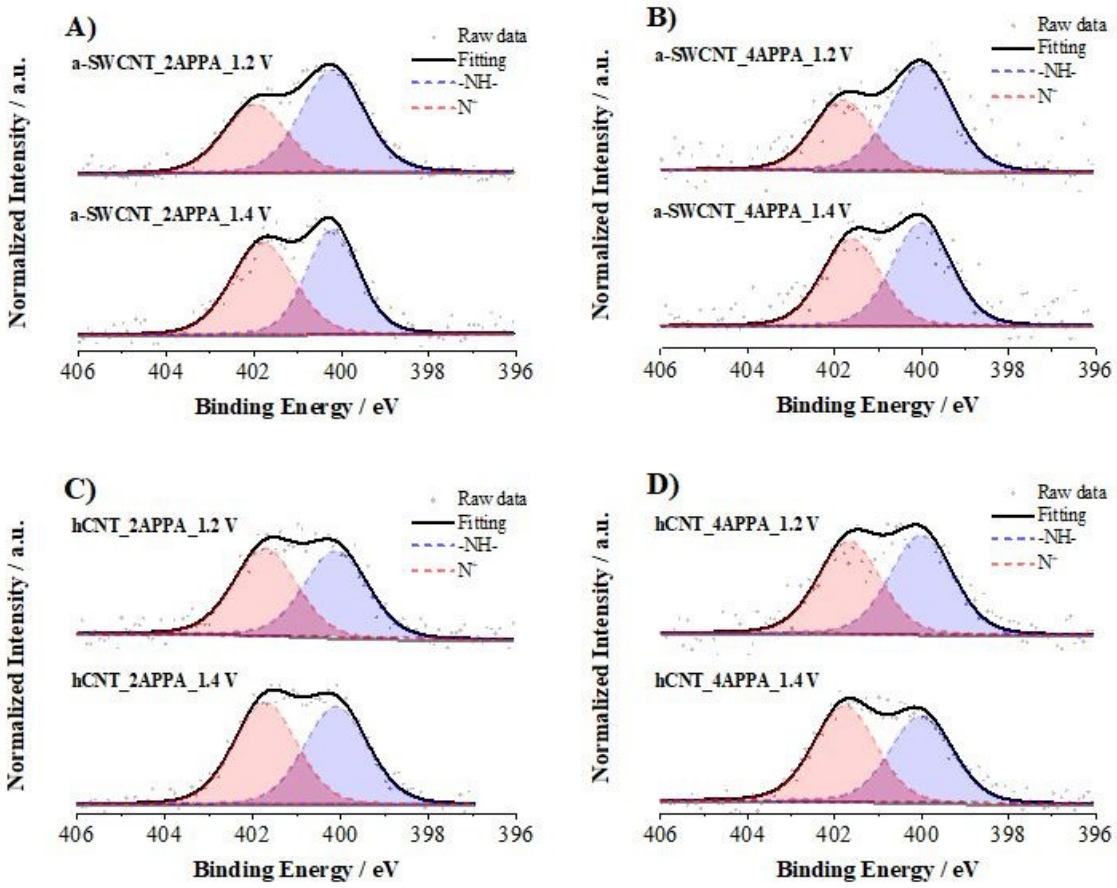

Figure 4. N1s spectra of: A, B) a-SWCNT and C, D) hCNT modified with A, C) 2APPA and B, D) 4APPA at 1.2 V and 1.4 V (vs RHE) determined by XPS.

The P2p spectra in Figure 5 reveal a main peak at around 133.5 – 134.0 eV that can be deconvoluted in one or two contributions composed of two asymmetric doublets. The first peak at 132.7 eV is characteristic of P-C species [85] and seems to be connected with the phosphonic groups from the APPA monomers. The second doublet, much more intense, lies at around 133.7 eV, in the range of binding energies related to P-O compounds [86], and it is probably ascribed to phosphate or phosphoric groups (R–O–$P(OH)_2$) produced during the electrochemical functionalization at oxidative conditions. It could be also possible for phosphonic groups to interact with carbon atoms through oxygen atoms. However, this trend is reversed when PANI-APPA copolymers are synthesized by chemical methods in the absence of carbon materials [84].

It is noteworthy that the P2p profiles for the CNTs modified with 2APPA shows only the contribution of more oxidized P atoms (Figures 5A and C). This is probably due to an increased reactivity of the phosphonic groups due to higher interactions between the phosphonic groups and the nitrogen species, which are favored in the linear 2APPA-related oligomers. Contrarily, the resulting branched structures with 4APPA seems to increase the resistance to oxidation of phosphorus atoms during the electrooxidation process. Figures S21 and S22 show the XPS full survey spectra, as well as the N1s and P2p spectra, respectively, for b-SWCNT electrochemically modified with both APPA monomers, revealing species similar to those of a-SWCNTs, but with less contribution of N^+ species when 2APPA is used. This behaviour corroborates different interactions between linear oligomers and a-SWCNTs surface, probably due to changes in their surface chemistry after treatment with the acid mixture. Additionally, Figures S23 and S24 display the XPS full survey spectra, as well as the N1s and P2p spectra, respectively, after the stability test, which reveal more changes for those CNTs modified with 4APPA than with 2APPA. This suggests that the interactions between the phosphorus and nitrogen groups in the linear 2APPA-related oligomers seems to stabilize their chemical environment under oxidative conditions.

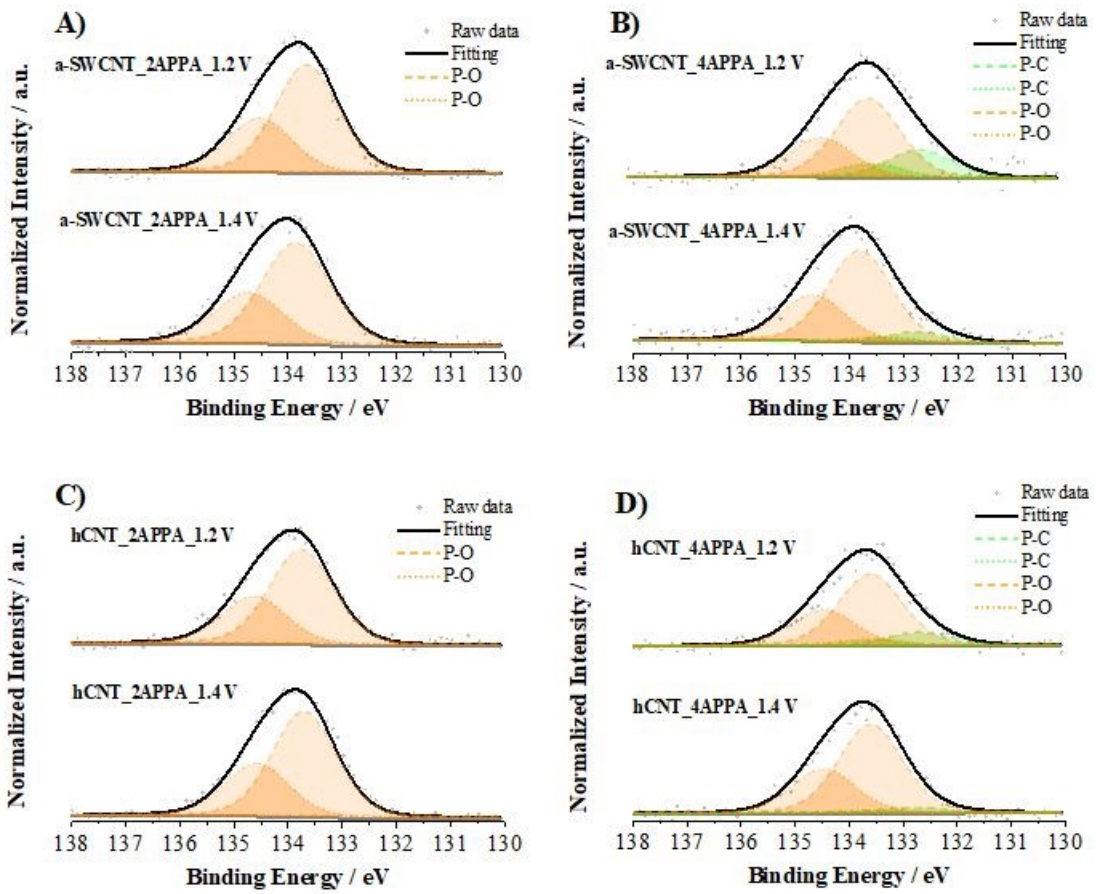

View Article Online
DOI: 10.1039/D1TA10322A

Figure 5. P2p spectra of: A, B) a-SWCNT and C, D) hCNT modified with A, C) 2APPA and B, D) 4APPA at 1.2 V and 1.4 V (vs RHE) determined by XPS.

Raman spectroscopy was used to study the physico-chemical and structural changes in the different CNTs before and after the electrochemical modification with 2APPA and 4APPA at different oxidation potentials. Figure 6 shows the most important characteristic features in the Raman spectra of graphene-based carbon materials, including the first-order G band and the disorder-induced D band at around 1570-1590 cm^{-1} and 1350 cm^{-1}, respectively [57,58]. An additional band of lower intensity can be clearly appreciated at around 1130 cm^{-1} after modifying the a-SWCNTs with both APPA monomers (Figure 6A and B), which could be ascribed to asymmetric C-N-C stretching mode in quinoid structures [34], C-H aromatic in-plane bending mode [84,87], as well as to P-O-C out-of-plane stretching in an aromatic system [34,88]. Therefore, the lack of this band in modified hCNTs confirms the non-favorable effect of this carbon structure for the oligomerization process. In this case, the inset images at Figures 6C and D reveal a shoulder of the G band at around 1620 cm^{-1} (D' band), which is sensitive to defects and strain induced in the graphene flakes by electrochemical functionalization and covalent interactions [58]. This is in agreement with the prevailing covalent attachment of APPA species in hCNTs through the numerous reactive sites and heterogeneities present in this material compared to a-SWCNT. In addition, when the anodic potential is increased in the modification process, a shift of the G band towards more positive wavenumbers is induced, probably due to covalent interactions with APPA monomers. This shift is especially noticed when hCNTs are modified with 4APPA (Figure 6D). Moreover, no significant differences are distinguished when comparing electrochemically modified a-SWCNTs (Figure 6A and B) with b-SWCNTs (Figure S25).

The I_D/I_G ratio was calculated by deconvolution of the D and G regions (Figures S26-S29), where the D and G bands have been fitted to Lorentzian curves [89,90]. The I_D/I_G ratio in Figure S30 reveals that a-SWCNTs modified at lower potentials do not present substantial structural damage, since the oxidation occurs mainly in the APPA monomers. Contrarily, hCNTs show considerably higher I_D/I_G ratio, which could be related to the covalent incorporation of functionalities that increases stacking defects. The I_D/I_G ratio comes to a maximum at around 1.4 V and 1.6 V. The maximum can be

explained considering that at more aggressive conditions (i.e., at higher potentials) some loss carbon material may occur, probably due to electrochemical gasification reactions [91]. Nonetheless, as seen in Figure S7 and S8 for ANI monomers, both the double-layer capacitance and pseudocapacitance contributions do not seem to be negatively affected up to higher potentials (1.6 and 1.8 V).

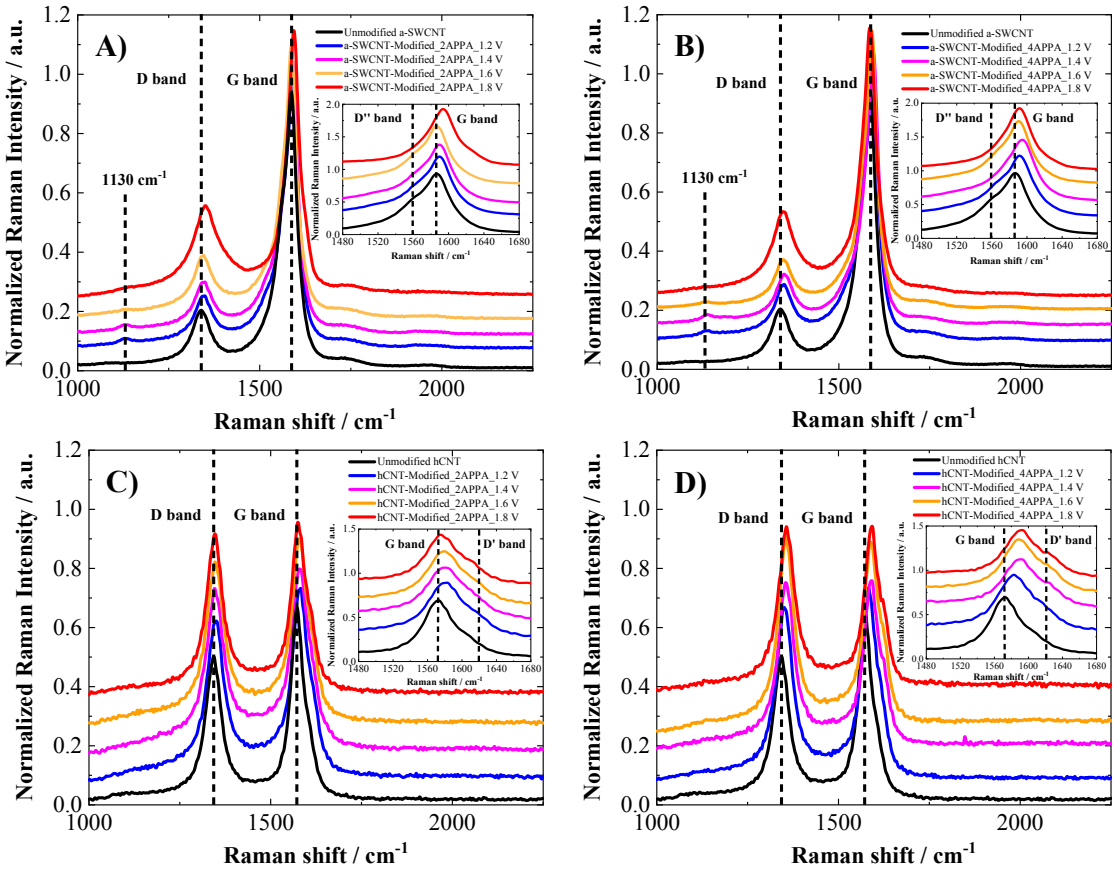

Figure 6. Raman spectra of A, B) a-SWCNT and C, D) hCNT electrochemically modified with A, C) 2APPA and B, D) 4APPA at different positive potentials. Inset: Enlargement of the D'', G and D' region.

View Article Online
DOI: 10.1039/D1TA10322A

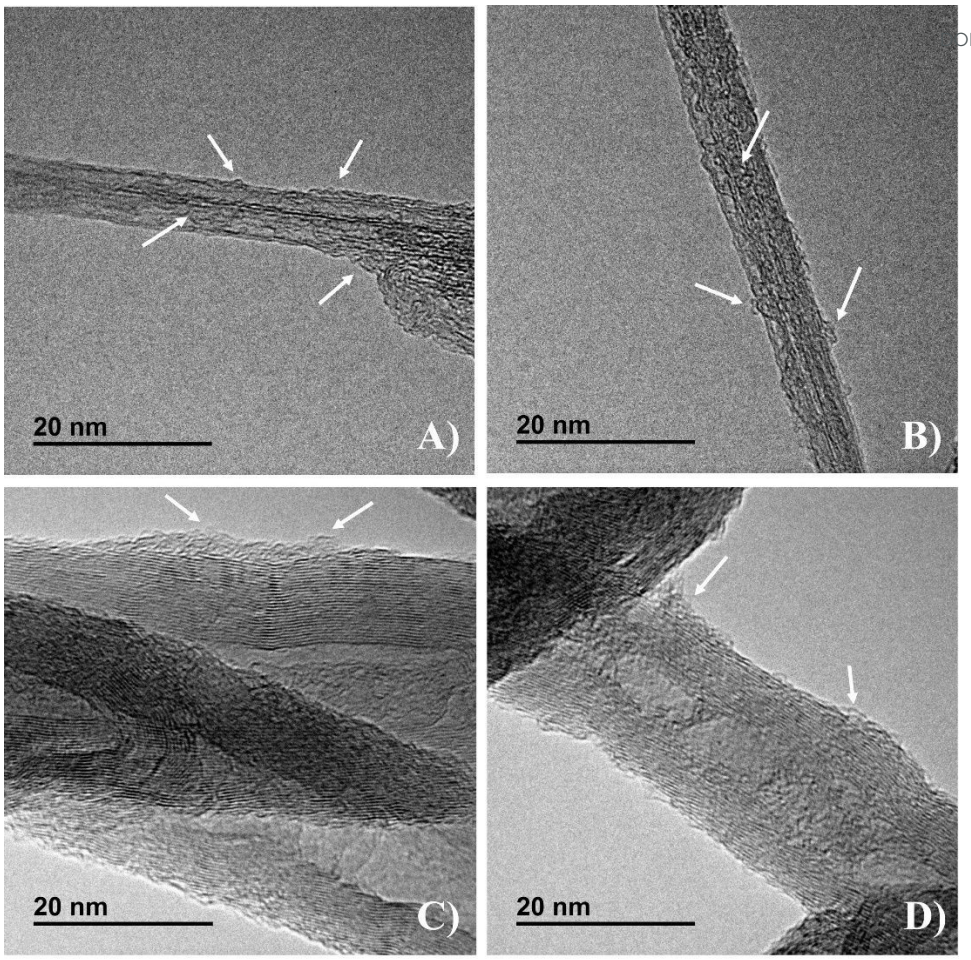

Figure 7. TEM images of A, B) a-SWCNT and C, D) hCNT electrochemically modified with A, C) 2APPA and B, D) 4APPA at 1.4 V (vs RHE).

Figure 7 displays the TEM images of the different CNTs electrochemically modified in presence of 2APPA and 4APPA, which can be compared with unmodified CNTs in Figure 1. The formation of amorphous material onto the surface of the CNT is observed (marked with white arrows), which is associated with the oligomers developed during the electrooxidation, especially in the case of a-SWCNTs (Figures 7A and B). These polymeric materials seem to be located not only on the outer surface of the nanotubes but also inside the channel of the nanotubes as a consequence of the opening of tips and some defective walls. Local attachment of radicals might take place at the most reactive sites, such as defects, edges or surface oxygen groups, followed by the development of oligomeric species [67]. Therefore, a heterogeneous and non-uniform oligomeric coating wraps the surface of CNTs in form of agglomerates with no apparent damage in their structure, suggesting that APPA monomers are preferentially oxidized rather than

the CNTs. It should be noted in Figures 7A and B that the functionalized a-SWCNTs generates more aggregates in comparison to functionalized b-SWCNTs and that the carbon nanotube channel in b-SWCNTs seems not to be filled (Figure S31), in agreement with the lack of CNT tip opening that occurs in this case. Besides, it is observed that a-SWCNTs modified with 4APPA give rise to few linear chains; however, loops due to inter- and intra-chain entanglements are observed, whereas 2APPA shows longer linear chains. Regarding the modified hCNTs (Figures 7C and D), the presence of amorphous material located at the edges and defect sites suggest their oxidation due to their high reactivity together with the anchoring of monomers or short-chain oligomers. However, as expected, oligomeric chains are less appreciable than with a-SWCNTs.

3.5. Density functional theory calculations (DFT)

The Self-Consistent Field (SCF) energy of the monomers and CNTs have been obtained for the evaluation of the energy involved in the functionalization mechanisms. A SWCNT with a (5,5) chiral vector and 0.7 nm of diameter was selected to model the mechanisms of the monomer adsorption. It is widely known that the electronic properties of carbon nanotubes highly depend on the chiral vector and diameter; however, by using the selected SWCNT model and B3LYP/6-31G(d) level of theory, a good balance between computational cost and high-quality results is reached. Nevertheless, as mentioned, the results obtained in this DFT calculation do not provide a general statement that can be applied to all carbon nanotubes, but give useful insights to better understand the interactions between SWCNT and the studied monomers.

Geometries of 2APPA, 4APPA and ANI have been optimized for 1, 2, 3 and 5 monomer-containing polymeric chains. Figure S32 displays the SCF energy per monomer units, in which an increase in the SCF energy is observed when increasing the number of monomers that form the polymer chain. Interestingly, slight differences can be observed depending on the monomer. 2APPA and ANI show similar SCF energy profiles for the whole range of monomer units, whereas in the case of 4APPA the required energy to continue with the polymerization is lower.

Figure S33 shows the optimized geometry for each monomer. It is observed that 5 monomers of 2APPA leads to a linear polymeric chain, similar to the obtained by the ANI, while 5 monomers of 4APPA result in a folded structure of the polymer chain as a

View Article Online
DOI: 10.1039/D1TA10322A

consequence of the interaction between -PO_3H_2 groups, which is in full agreement with TEM observations. The *para*- disposition of the phosphonic groups in 4APPA-based chains leads to a configuration in which the phosphonic groups are found closer than in 2APPA-based chains. This results in the interaction between the P-containing functional groups of different monomers that decreases the polymerization energy. These computational results provide important information about the experimental differences of 2APPA and 4APPA polymerization and the electrochemical and physicochemical properties since the chain structure determines many properties, such as the electrical conductivity. The modelling is in excellent agreement with the experimental assumptions, in which the molecules adsorbed on the CNTs are mainly related to polymeric species characteristic of the first stages of ANI polymerization, especially 4ADPA dimers or short oligomeric-related chains in the case of 2APPA, and more branched species related to PhzR-type structures and derivatives in the presence of 4APPA.

Furthermore, the adsorption energies of ANI, 2APPA and 4APPA on the outer surface of carbon nanotubes have also been evaluated (Figure 8 and Table 2). The model structures and computational details can be found in the experimental section. It should be noted that, despite recent theoretical studies have indicated preferences in the intermolecular interaction of aromatic molecules on the inner surface of the CNTs [44], this configuration has not been studied due to the small diameter associated to them in order to obtain adequate calculation times in this fundamental study. Nevertheless, it is important to consider this possibility, especially in the case of a-SWCNTs, since experimental results have demonstrated the opening of the tips and the availability of the internal surface for their functionalization, as seen in TEM images (Figure 7).

Two possible orientations have been considered for modelling the interaction of a-SWCNT with ANI and APPA-based monomers: parallel and perpendicular to the longitudinal axis of the nanotube. However, only parallel configuration was found to be stable, probably due to interactions of the π electrons of the CNTs and the hydrogen atoms of the N and P groups. Moreover, π-π interactions can also be possible from the π electrons of the CNTs and the benzene rings. One aspect that must be pointed out is the different adsorption energies depending on the monomer. The adsorption energy for aniline is found to be -39.28 kJ mol^{-1}, while the adsorption energy for both APPA-based monomers is significantly more negative, showing a stronger interaction between

View Article Online
DOI: 10.1039/D1TA10322A

2APPA and 4APPA and the carbon nanotube. This can be explained through an interaction between the P-containing functional group and the nanotubes walls. If the CNTs are oxidized (as it occurs for a-SWCNT), the interaction seems to be stronger for ANI and 4APPA with respect to the non-oxidized SWCNTs, although the higher values are found for APPA monomers (Figure 8 and Table 2).

From these values, it can be deduced that the interaction of 2APPA is more likely to occur on the CNTs through π-π interactions and the linear polymeric growth of the chain could easily occur (as with ANI), whereas 4APPA-derived polymer has no relevant π-π interactions with the CNTs due to the folded structure (Figure S33) and thus the polymerization along the CNTs surface is hampered. Therefore, in the last case, the radical 4APPA* that act as nucleation point can be formed at parallel position to the CNTs, but the growth is highly hampered due to the non-linear structure. Thus, the polymerization of 4APPA can likely occur in solution and then deposited on the carbon nanotube surface, so the proportion of oligomers and the size of the chains must be smaller, in agreement with the lower N content of 4APPA functionalization in XPS results.

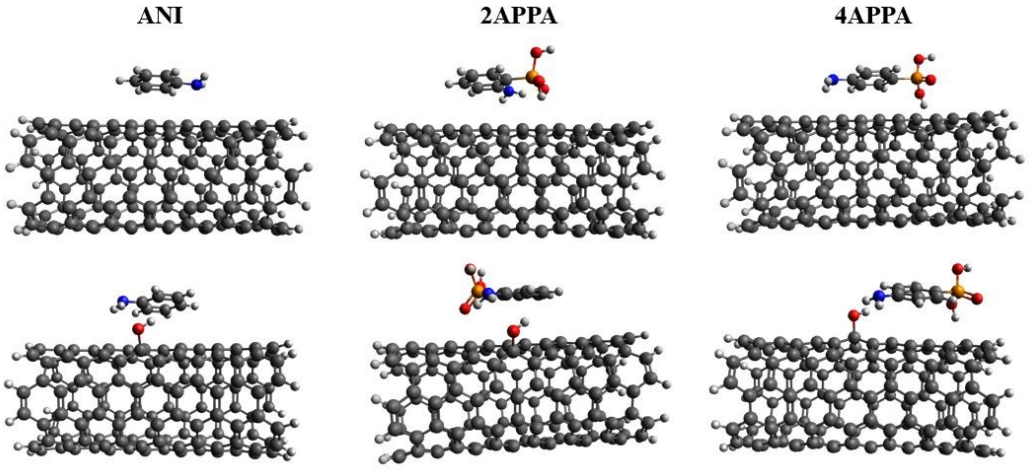

Figure 8. Optimized geometries for the adsorption of ANI, 2APPA and 4APPA in SWCNTs and oxidized SWCNTs. H is white, C is grey, N is blue, O is red, and P is orange.

Table 2. Adsorption energies for ANI, 2APPA and 4APPA monomers onto SWCNTs and oxidized SWCNTs.

CNT type	Adsorption energy / kJ mol^{-1}

View Article Online
DOI: 10.1039/D1TA10322A

	ANI	2APPA	4APPA
SWCNT	-39.28	-86.21	-81.51
Oxidized SWCNT	-68.60	-80.22	-101.07

Additionally, the adsorption of ANI and APPA monomers in hCNTs have been modelled through the adsorption energies at the edges of the carbon nanotube in order to deepen into the differences between both CNTs structures. To that end, Figure 9 and Table 3 show the optimized geometries and SCF energies of the adsorption of all monomers, respectively. Interestingly, in comparison with the SCF energies obtained at the basal plane (Figure 8 and Table 2), the adsorption energies of ANI, 2APPA and 4APPA are significantly higher in this modelling, which means a stronger interaction of monomers in the edges of carbon nanotubes (as in hCNTs), what is especially remarkable when CNTs are oxidized. It is worth mentioning that ANI tends to enter into the carbon nanotube, possibly due to high adsorption potential through the π-π interaction. In this regard, the optimized geometries shown in Figure 9 seem to indicate the APPA monomers mainly interact with the edges and the oxygen group through the P-containing functional group. However, experimentally we have observed that the electrooxidation of APPA monomers in presence of hCNTs leads to smaller redox processes in CV profiles in comparison with a-SWCNTs (see Figure 3). This means that despite the higher functionalization degree of hCNTs (detected by XPS, see Table 1), the APPA-derived functional groups do not form a polymer-like functionalization with the polyaniline-type characteristic redox processes and it is mainly limited to covalent attachment of monomers.

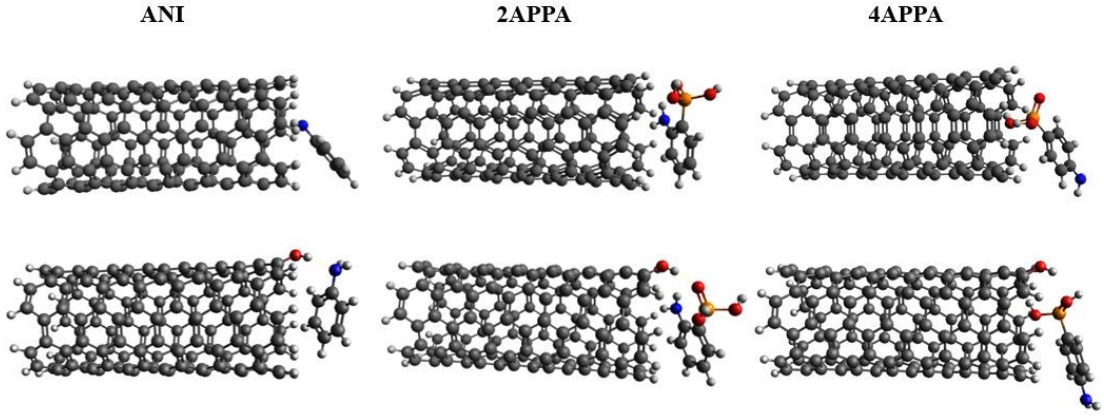

Figure 9. Optimized geometries for the adsorption of ANI, 2APPA and 4APPA at the edges of SWCNTs and oxidized SWCNTs. H is white, C is grey, N is blue, O is red, and P is orange.

View Article Online
DOI: 10.1039/D1TA10322A

Table 3. Adsorption energies for ANI, 2APPA and 4APPA monomers at the edges of SWCNTs and oxidized SWCNTs.

CNT type	Adsorption energy / kJ mol^{-1}		
	ANI	2APPA	4APPA
SWCNT	-69.73	-87.93	-107.21
Oxidized SWCNT	-85.29	-123.86	-127.38

According to these results, it is suggested that in presence of hCNTs, in which edges predominate, APPA monomers tend to react more strongly with the carbon atoms located at the edges of the carbon nanotubes, probably through covalent bonding and such strong interaction does not allow the polymerization reaction. However, in presence of a-SWCNTs, in which basal plane atoms predominate, the interaction with APPA monomers occur through weaker (but favorable) physical phenomena, which does allow the oligomeric growth.

4. Conclusions

The electrochemical functionalization of SWCNTs and hCNTs has been carried out in presence of aminophenylphosphonic acid isomers (2APPA or 4APPA), with an excellent level of control regarding the N and P species incorporated. Interestingly, a-SWCNTs seem to favor the correct adsorption of the monomers onto the CNTs wall through interaction with the π electrons of the walls, followed by the oligomeric growth, while hCNTs promote a covalent attachment of the monomers and short-chains formation according to their heterogeneity and higher reactivity, where a high functionalization level can be reached but the development of polymers is not favored. Local attachment of radicals could take place at the most reactive sites, giving rise to a heterogeneous distribution of functionalities with no apparent damage in the structure of CNTs.

Not only the structure of CNTs, but also the position of the phosphonic groups in the monomer are key factors for the resultant polymer formation and its electrochemical stability. Hence, the functionalization in presence of 2APPA reveals similar electrochemical profiles to the modification in presence of ANI under the same

conditions since linear chain growth is expected. Nevertheless, when 4APPA is used, the resulting oligomers show folded structures that impede their growth on the CNTs wall. Modelling results support these findings and help us to gain a deeper understanding of the functionalization mechanism of CNTs with different structures. Therefore, modification of CNTs with 2APPA provides a higher presence of N and P heteroatoms under the optimal conditions (1.2 and 1.4 V vs RHE), which can be a promising methodology to develop electrocatalysts and electrocatalysts support for next-generation electrochemical energy devices.

Author Contributions

The paper was planned and written with contributions from all authors. All authors have read and agreed to the published version of the manuscript.

Conflicts of Interest

The authors declare no conflict of interest.

Acknowledgments

B.M.-S. thanks the Ministry of Science, Innovation and Universities of Spain for the FPU grant (FPU18/05127). The authors would like to thank MICINN and FEDER (projects PID2019-105923RB-100 and RTI2018-095291-B-I00) for the financial support.

References

[1] M. Inagaki, F. Kang, M. Toyoda, H. Konno, Advanced Materials Science and Engineering of Carbon, 1st ed. Elsevier, Tsinghua, China, 2014. doi: https://doi.org/10.1557/mrs.2014.271.

[2] H. Macpherson, “Nanocarbons for Energy Conversion: Supramolecular Approaches”, 1st ed. Springer International Publishing, Japan, 2019. doi:10.1595/205651319x15662086564793.

[3] N. Arora, N.N. Sharma, Arc discharge synthesis of carbon nanotubes: Comprehensive review, Diam. Relat. Mater. 50 (2014) 135–150. doi:https://doi.org/10.1016/j.diamond.2014.10.001.

[4] C.D. Scott, S. Arepalli, P. Nikolaev, R.E. Smalley, Growth mechanisms for single-wall carbon nanotubes in a laser-ablation process, Appl. Phys. A. 72 (2001) 573–580. doi:10.1007/s003390100761.

[5] F. Danafar, A. Fakhru'l-Razi, M.A.M. Salleh, D.R.A. Biak, Fluidized bed catalytic chemical vapor deposition synthesis of carbon nanotubes—A review, Chem. Eng. J. 155 (2009) 37–48. doi:https://doi.org/10.1016/j.cej.2009.07.052.

[6] L. Zhang, L. Chen, T. Wells, M. El-Gomati, Bamboo and herringbone shaped carbon nanotubes and carbon nanofibres synthesized in direct current-plasma enhanced chemical vapour deposition, J. Nanosci. Nanotechnol. 9 (2009) 4502–4506. doi:10.1166/jnn.2009.M84.

[7] D. Vairavapandian, P. Vichchulada, M.D. Lay, Preparation and modification of carbon nanotubes: Review of recent advances and applications in catalysis and sensing, Anal. Chim. Acta. 626 (2008) 119–129. doi:https://doi.org/10.1016/j.aca.2008.07.052.

[8] E. Salernitano, L. Giorgi, T. Dikonimos Makris, R. Giorgi, N. Lisi, V. Contini, M. Falconieri, Purification of MWCNTs grown on a nanosized unsupported Fe-based powder catalyst, Diam. Relat. Mater. 16 (2007) 1565–1570. doi:10.1016/j.diamond.2006.12.038.

[9] P. Vichchulada, J. Shim, M.D. Lay, Non-oxidizing Purification Method for Large Volumes of Long, Undamaged Single-Walled Carbon Nanotubes, J. Phys. Chem. C. 112 (2008) 19186–19192. doi:10.1021/jp803989d.

[10] V. Đorđević, J. Djustebek, J. Cveticanin, S. Velickovic, M. Veljkovic, M. Bokorov, B. Babić-Stojić, O. Neskovic, Methods of Purification and Characterization of Carbon Nanotubes, J. Optoelectron. Adv. Mater. 8 (2006) 1631–1634.

[11] C. Vix-Guterl, M. Couzi, J. Dentzer, M. Trinquecoste, P. Delhaes, Surface Characterizations of Carbon Multiwall Nanotubes: Comparison between Surface Active Sites and Raman Spectroscopy, J. Phys. Chem. B. 108 (2004) 19361–19367. doi:10.1021/jp047237s.

[12] A.C. Dillon, T. Gennett, K.M. Jones, J.L. Alleman, P.A. Parilla, M.J. Heben, A Simple and Complete Purification of Single-Walled Carbon Nanotube Materials, Adv. Mater. 11 (1999) 1354–1358. doi:10.1002/(SICI)1521-4095(199911)11:16<1354::AID-

View Article Online
DOI: 10.1039/D1TA10322A

ADMA1354>3.0.CO;2-N.

[13] A. Hirsch, O. Vostrowsky, Functionalization of Carbon Nanotubes, in: A.D. Schlüter (Ed.), Springer Berlin Heidelberg, Berlin, Heidelberg, 2005: pp. 193–237. doi:10.1007/b98169.

[14] V.N. Khabashesku, Covalent functionalization of carbon nanotubes: synthesis, properties and applications of fluorinated derivatives, Russ. Chem. Rev. 80 (2011) 705–725. doi:10.1070/rc2011v080n08abeh004232.

[15] P. Bilalis, D. Katsigiannopoulos, A. Avgeropoulos, G. Sakellariou, Non-covalent functionalization of carbon nanotubes with polymers, RSC Adv. 4 (2014) 2911–2934. doi:10.1039/C3RA44906H.

[16] T. Fujigaya, N. Nakashima, Non-covalent polymer wrapping of carbon nanotubes and the role of wrapped polymers as functional dispersants, Sci. Technol. Adv. Mater. 16 (2015) 24802. doi:10.1088/1468-6996/16/2/024802.

[17] C.-Y. Hu, Y.-J. Xu, S.-W. Duo, R.-F. Zhang, M.-S. Li, Non-Covalent Functionalization of Carbon Nanotubes with Surfactants and Polymers, J. Chinese Chem. Soc. 56 (2009) 234–239. doi:10.1002/jccs.200900033.

[18] S.N. Jaisankar, N. Haridharan, A. Murali, P. Sergii, M. Špírková, A.B. Mandal, L. Matějka, Single-electron transfer living radical copolymerization of SWCNT-g-PMMA via graft from approach, Polymer. 55 (2014) 2959–2966. doi:https://doi.org/10.1016/j.polymer.2014.04.054.

[19] F.A. Abuilaiwi, T. Laoui, M. Al-Harthi, M.A. Atieh, Modification and functionalization of multiwalled carbon nanotube (MWCNT) via fischer esterification, Arab. J. Sci. Eng. 35 (2010) 37–48.

[20] L. Meng, C. Fu, Q. Lu, Advanced technology for functionalization of carbon nanotubes, Prog. Nat. Sci. 19 (2009) 801–810. doi:https://doi.org/10.1016/j.pnsc.2008.08.011.

[21] E. Del Canto, K. Flavin, D. Movia, C. Navio, C. Bittencourt, S. Giordani, Critical investigation of defect site functionalization on single-walled carbon nanotubes, Chem. Mater. 23 (2011) 67–74. doi:10.1021/cm101978m.

[22] D. Tasis, N. Tagmatarchis, A. Bianco, M. Prato, Chemistry of carbon nanotubes, Chem. Rev. 106 (2006) 1105–1136. doi:10.1021/cr050569o.

[23] C. Oueiny, S. Berlioz, F.-X. Perrin, Carbon nanotube–polyaniline composites, Prog. Polym. Sci. 39 (2014) 707–748. doi:https://doi.org/10.1016/j.progpolymsci.2013.08.009.

[24] T. Zhang, M.B. Nix, B.-Y. Yoo, M.A. Deshusses, N.V. Myung, Electrochemically Functionalized Single-Walled Carbon Nanotube Gas Sensor, Electroanalysis. 18 (2006) 1153–1158. doi:10.1002/elan.200603527.

[25] A. Gabe, M.J. Mostazo-López, D. Salinas-Torres, E. Morallón, D. Cazorla-Amorós, Synthesis of conducting polymer/carbon material composites and their application in electrical energy storage, in: Hybrid Polym. Compos. Mater., Elsevier, 2017: pp. 173–209. doi:10.1016/B978-0-08-100789-1.00008-3.

[26] C. González-Gaitán, R. Ruiz-Rosas, E. Morallón, D. Cazorla-Amorós, Electrochemical Methods to Functionalize Carbon Materials, in: V.K. Thakur, M.K. Thakur (Eds.), Chem. Funct. Carbon Nanomater. Chem. Appl., CRC Press, Taylor & Francis Groups, 2016: pp. 231–262.

[27] C. González-Gaitán, R. Ruiz-Rosas, E. Morallón, D. Cazorla-Amorós, Functionalization of carbon nanotubes using aminobenzene acids and electrochemical methods. Electroactivity for the oxygen reduction reaction, Int. J. Hydrogen Energy. 40 (2015) 11242–11253. doi:https://doi.org/10.1016/j.ijhydene.2015.02.070.

[28] D. Yu, Y. Xue, L. Dai, Vertically Aligned Carbon Nanotube Arrays Co-doped with Phosphorus and Nitrogen as Efficient Metal-Free Electrocatalysts for Oxygen Reduction, J. Phys. Chem. Lett. 3 (2012) 2863–2870. doi:10.1021/jz3011833.

[29] A. Abellán-Llobregat, C. González-Gaitán, L. Vidal, A. Canals, E. Morallón, Portable electrochemical sensor based on 4-aminobenzoic acid-functionalized herringbone carbon nanotubes for the determination of ascorbic acid and uric acid in human fluids, Biosens. Bioelectron. 109 (2018) 123–131. doi:https://doi.org/10.1016/j.bios.2018.02.047.

[30] C. González-Gaitán, R. Ruiz-Rosas, E. Morallón, D. Cazorla-Amorós, Effects of the surface chemistry and structure of carbon nanotubes on the coating of glucose oxidase and electrochemical biosensors performance, RSC Adv. 7 (2017) 26867–26878. doi:10.1039/c7ra02380d.

[31] J.P. Paraknowitsch, A. Thomas, Doping carbons beyond nitrogen: an overview of advanced heteroatom doped carbons with boron, sulphur and phosphorus for energy applications, Energy Environ. Sci. 6 (2013) 2839–2855. doi:10.1039/C3EE41444B.

[32] A.F. Quintero-Jaime, D. Cazorla-Amorós, E. Morallón, Electrochemical functionalization of single wall carbon nanotubes with phosphorus and nitrogen species, Electrochim. Acta. 340 (2020) 135935. doi:https://doi.org/10.1016/j.electacta.2020.135935.

[33] A.F. Quintero-Jaime, F. Conzuelo, W. Schuhmann, D. Cazorla-Amorós, E. Morallón, Multi-wall carbon nanotubes electrochemically modified with phosphorus and nitrogen functionalities as a basis for bioelectrodes with improved performance, Electrochim. Acta. 387 (2021) 138530. doi:10.1016/j.electacta.2021.138530.

[34] A.F. Quintero-Jaime, D. Cazorla-Amorós, E. Morallón, Effect of surface oxygen groups in the electrochemical modification of multi-walled carbon nanotubes by 4-amino phenyl phosphonic acid, Carbon. 165 (2020) 328–339. doi:10.1016/j.carbon.2020.04.062.

[35] O. Ornelas, J.M. Sieben, R. Ruiz-Rosas, E. Morallón, D. Cazorla-Amorós, J. Geng, N. Soin, E. Siores, B.F.G. Johnson, On the origin of the high capacitance of nitrogen-containing carbon nanotubes in acidic and alkaline electrolytes, Chem. Commun. 50 (2014) 11343–11346. doi:10.1039/c4cc04876h.

[36] A. Benyoucef, F. Huerta, J.L. Vázquez, E. Morallon, Synthesis and in situ FTIRS characterization of conducting polymers obtained from aminobenzoic acid isomers at platinum electrodes, Eur. Polym. J. 41 (2005) 843–852. doi:10.1016/j.eurpolymj.2004.10.047.

[37] C. Sanchís, H.J. Salavagione, J. Arias-Pardilla, E. Morallón, Tuning the electroactivity of conductive polymer at physiological pH, Electrochim. Acta. 52 (2007) 2978–2986. doi:https://doi.org/10.1016/j.electacta.2006.09.031.

[38] H.J. Salavagione, J. Arias, P. Garcés, E. Morallón, C. Barbero, J.L. Vázquez, Spectroelectrochemical study of the oxidation of aminophenols on platinum electrode in acid medium, J. Electroanal. Chem. 565 (2004) 375–383. doi:https://doi.org/10.1016/j.jelechem.2003.11.005.

[39] J. Masa, A. Zhao, W. Xia, Z. Sun, B. Mei, M. Muhler, W. Schuhmann, Trace metal residues promote the activity of supposedly metal-free nitrogen-modified carbon catalysts for the oxygen reduction reaction, Electrochem. Commun. 34 (2013) 113–116. doi:10.1016/j.elecom.2013.05.032.

[40] C. Liu, H.-M. Cheng, Carbon nanotubes: controlled growth and application, Mater. Today. 16 (2013) 19–28. doi:10.1016/j.mattod.2013.01.019.

[41] M. Filchakova, V. Saik, Single-walled carbon nanotubes: structure, properties, applications, and health & safety, (2021). https://tuball.com/articles/single-walled-carbon-nanotubes (accessed February 8, 2022).

[42] A. Gabe, R. Ruiz-Rosas, E. Morallón, D. Cazorla-Amorós, Understanding of oxygen reduction reaction by examining carbon-oxygen gasification reaction and carbon active

sites on metal and heteroatoms free carbon materials of different porosities and structures, Carbon. 148 (2019) 430–440. doi:https://doi.org/10.1016/j.carbon.2019.03.092.

[43] C. Shen, A.H. Brozena, Y. Wang, Double-walled carbon nanotubes: Challenges and opportunities, Nanoscale. 3 (2011) 503–518. doi:10.1039/C0NR00620C.

[44] D.H. Ahn, C. Park, J.W. Song, Predicting whether aromatic molecules would prefer to enter a carbon nanotube: A density functional theory study, J. Comput. Chem. 41 (2020) 1261–1270. doi:10.1002/jcc.26173.

[45] C. Rajesh, C. Majumder, H. Mizuseki, Y. Kawazoe, A theoretical study on the interaction of aromatic amino acids with graphene and single walled carbon nanotube, J. Chem. Phys. 130 (2009) 124911. doi:10.1063/1.3079096.

[46] M. Smeu, F. Zahid, W. Ji, H. Guo, M. Jaidann, H. Abou-Rachid, Energetic molecules encapsulated inside carbon nanotubes and between graphene layers: DFT calculations, J. Phys. Chem. C. 115 (2011) 10985–10989. doi:10.1021/jp201756p.

[47] J.L. Figueiredo, M.F.R. Pereira, M.M.A. Freitas, J.J.M. Órfão, Modification of the surface chemistry of activated carbons, Carbon. 37 (1999) 1379–1389. doi:10.1016/S0008-6223(98)00333-9.

[48] K.I. Ramachandran, G. Deepa, K. Namboori, Computational Chemistry and Molecular Modeling, Springer Berlin Heidelberg, Berlin, Heidelberg, 2008. doi:10.1007/978-3-540-77304-7.

[49] A.D. Becke, Density-functional thermochemistry. III. The role of exact exchange, J. Chem. Phys. 98 (1993) 5648–5652. https://doi.org/10.1063/1.464913.

[50] C. Lee, W. Yang, R.G. Parr, Development of the Colle-Salvetti correlation-energy formula into a functional of the electron density, Phys. Rev. B. 37 (1988) 785–789. https://doi.org/10.1103/PhysRevB.37.785.

[51] W.J. Hehre, R. Ditchfield, J.A. Pople, Self-Consistent Molecular Orbital Methods. XII. Further Extensions of Gaussian-Type Basis Sets for Use in Molecular Orbital Studies of Organic Molecules, J. Chem. Phys. 56 (1972) 2257–2261. https://doi.org/10.1063/1.1677527.

[52] P.C. Hariharan, J.A. Pople, The influence of polarization functions on molecular orbital hydrogenation energies, Theor. Chim. Acta. 28 (1973) 213–222. https://doi.org/10.1007/BF00533485.

[53] M.J. Frisch, G.W. Trucks, H.B. Schlegel, G.E. Scuseria, M.A. Robb, J.R. Cheeseman, G. Scalmani, V. Barone, G.A. Petersson, H. Nakatsuji, Gaussian Development Version, revision I. 13; Gaussian, Inc, Wallingford, CT, USA, 2016.

[54] S. Grimme, A. Hansen, J.G. Brandenburg, C. Bannwarth, Dispersion-Corrected Mean-Field Electronic Structure Methods, Chem. Rev. 116 (2016) 5105–5154. doi:10.1021/acs.chemrev.5b00533.

[55] J. Hodkiewicz, Characterizing Carbon Materials with Raman Spectroscopy -application note, Thermo Fish. Sci. (2010) 1–5. http://thermo.com.

[56] A. Santidrián, J.M. González-Domínguez, V. Diez-Cabanes, J. Hernández-Ferrer, W.K. Maser, A.M. Benito, A. Anśon-Casaos, J. Cornil, T. Da Ros, M. Kalbáč, A tool box to ascertain the nature of doping and photoresponse in single-walled carbon nanotubes, Phys. Chem. Chem. Phys. 21 (2019) 4063–4071. doi:10.1039/c8cp06961a.

[57] M.S. Dresselhaus, A. Jorio, A.G. Souza Filho, R. Saito, Defect characterization in graphene and carbon nanotubes using Raman spectroscopy, Philos. Trans. R. Soc. A Math. Phys. Eng. Sci. 368 (2010) 5355–5377. doi:10.1098/rsta.2010.0213.

[58] H.J. Salavagione, P.S. Shuttleworth, J.P. Fernández-Blázquez, G.J. Ellis, M.A. Gómez-Fatou, Scalable graphene-based nanocomposite coatings for flexible and washable conductive textiles, Carbon. 167 (2020) 495–503. doi:10.1016/j.carbon.2020.05.108.

[59] J.H. Lehman, M. Terrones, E. Mansfield, K.E. Hurst, V. Meunier, Evaluating the characteristics of multiwall carbon nanotubes, Carbon. 49 (2011) 2581–2602. doi:10.1016/j.carbon.2011.03.028.

[60] D. Salinas-Torres, F. Huerta, F. Montilla, E. Morallón, Study on electroactive and electrocatalytic surfaces of single walled carbon nanotube-modified electrodes, Electrochim. Acta. 56 (2011) 2464–2470. doi:10.1016/j.electacta.2010.11.023.

[61] Y. Zhang, Z. Shi, Z. Gu, S. Iijima, Structure modification of single-wall carbon nanotubes, Carbon. 38 (2000) 2055–2059. doi:10.1016/S0008-6223(00)00047-6.

[62] C. Domingo, G. Santoro, Espectroscopía Raman de nanotubos de carbono, Opt. Pura y Apl. 40 (2007) 175–186.

[63] M.J. Bleda-Martínez, D. Lozano-Castelló, E. Morallón, D. Cazorla-Amorós, A. Linares-Solano, Chemical and electrochemical characterization of porous carbon materials, Carbon. 44 (2006) 2642–2651. doi:10.1016/j.carbon.2006.04.017.

[64] J. Zhang, H. Zou, Q. Qing, Y. Yang, Q. Li, Z. Liu, X. Guo, Z. Du, Effect of Chemical

Oxidation on the Structure of Single-Walled Carbon Nanotubes, J. Phys. Chem. B. 107 (2003) 3712–3718. doi:10.1021/jp027500u.

[65] R. Sharma, J.H. Baik, C.J. Perera, M.S. Strano, Anomalously Large Reactivity of Single Graphene Layers and Edges toward Electron Transfer Chemistries, Nano Lett. 10 (2010) 398–405. doi:10.1021/nl902741x.

[66] H. Yang, A.J. Bard, The application of fast scan cyclic voltammetry. Mechanistic study of the initial stage of electropolymerization of aniline in aqueous solutions, J. Electroanal. Chem. 339 (1992) 423–449.

[67] S.E. Kooi, U. Schlecht, M. Burghard, K. Kern, Electrochemical modification of single carbon nanotubes, Angew. Chemie - Int. Ed. 41 (2002) 1353–1355. doi:10.1002/1521-3773(20020415)41:8<1353::AID-ANIE1353>3.0.CO;2-I.

[68] M. Baibarac, I. Baltog, S. Lefrant, J.Y. Mevellec, O. Chauvet, Polyaniline and Carbon Nanotubes Based Composites Containing Whole Units and Fragments of Nanotubes, Chem. Mater. 15 (2003) 4149–4156. doi:10.1021/cm021287x.

[69] L.R. Radovic, I.F. Silva, J.I. Ume, J.A. Menéndez, C.A. Leon Y Leon, A.W. Scaroni, An experimental and theoretical study of the adsorption of aromatics possessing electron-withdrawing and electron-donating functional groups by chemically modified activated carbons, Carbon. 35 (1997) 1339–1348. doi:10.1016/S0008-6223(97)00072-9.

[70] L. Duić, Z. Mandić, S. Kovač, Polymer-dimer distribution in the electrochemical synthesis of polyaniline, Electrochim. Acta. 40 (1995) 1681–1688. doi:https://doi.org/10.1016/0013-4686(95)00086-T.

[71] G.A. Planes, J.L. Rodríguez, M.C. Miras, G. García, E. Pastor, C.A. Barbero, Spectroscopic evidence for intermediate species formed during aniline polymerization and polyaniline degradation, Phys. Chem. Chem. Phys. 12 (2010) 10584–10593. doi:10.1039/c002920c.

[72] E.M. Geniès, M. Lapkowski, J.F. Penneau, Cyclic voltammetry of polyaniline: interpretation of the middle peak, J. Electroanal. Chem. 249 (1988) 97–107. doi:10.1016/0022-0728(88)80351-6.

[73] A.N. Kuznetsov, A.B. Ayupov, P.M. Yeletsky, M. V. Lebedeva, Influence of monomer content on course of aniline polymerization in presence of high surface area carbon, J. Electroanal. Chem. 835 (2019) 73–80. doi:10.1016/j.jelechem.2018.12.057.

[74] D. Salinas-Torres, J.M. Sieben, D. Lozano-Castelló, D. Cazorla-Amorós, E. Morallón, Asymmetric hybrid capacitors based on activated carbon and activated carbon fibre-

PANI electrodes, Electrochim. Acta. 89 (2013) 326–332. doi:10.1016/j.electacta.2012.11.039.

[75] A. Kellenberger, E. Dmitrieva, L. Dunsch, The stabilization of charged states at phenazine-like units in polyaniline under p-doping: An in situ ATR-FTIR spectroelectrochemical study, Phys. Chem. Chem. Phys. 13 (2011) 3411–3420. doi:10.1039/c0cp01264e.

[76] Z. Ding, T. Sanchez, A. Labouriau, S. Iyer, T. Larson, R. Currier, Y. Zhao, D. Yang, Characterization of reaction intermediate aggregates in aniline oxidative polymerization at low proton concentration, J. Phys. Chem. B. 114 (2010) 10337–10346. doi:10.1021/jp102623z.

[77] R. Berenguer, R. Ruiz-Rosas, A. Gallardo, D. Cazorla-Amorós, E. Morallón, H. Nishihara, T. Kyotani, J. Rodríguez-Mirasol, T. Cordero, Enhanced electro-oxidation resistance of carbon electrodes induced by phosphorus surface groups, Carbon. 95 (2015) 681–689. doi:10.1016/j.carbon.2015.08.101.

[78] C. González-Gaitán, R. Ruiz-Rosas, H. Nishihara, T. Kyotani, E. Morallón, D. Cazorla-Amorós, Successful functionalization of superporous zeolite templated carbon using aminobenzene acids and electrochemical methods, Carbon. 99 (2016) 157–166. doi:10.1016/j.carbon.2015.12.006.

[79] S.N. Kumar, G. Bouyssoux, F. Gaillard, Electronic and structural characterization of electrochemically synthesized conducting polyaniline from XPS studies, Surf. Interface Anal. 15 (1990) 531–536. doi:10.1002/sia.740150906.

[80] E.T. Kang, K.G. Neoh, K.L. Tan, The intrinsic redox states in polypyrrole and polyaniline: A comparative study by XPS, Surf. Interface Anal. 19 (1992) 33–37. doi:10.1002/sia.740190110.

[81] M.J. Mostazo-López, R. Ruiz-Rosas, E. Morallón, D. Cazorla-Amorós, Generation of nitrogen functionalities on activated carbons by amidation reactions and Hofmann rearrangement: Chemical and electrochemical characterization, Carbon. 91 (2015) 252–265. https://doi.org/10.1016/j.carbon.2015.04.089.

[82] T. Remyamol, H. John, P. Gopinath, Phenylene diamine mediated covalent grafting of polyaniline on reduced graphene oxide for optical Limiting, in: Int. Conf. Adv. Nanomater. Emerg. Eng. Technol., IEEE, 2013: pp. 204–207. https://doi.org/10.1109/ICANMEET.2013.6609277.

[83] T. Amaya, I. Kurata, Y. Inada, T. Hatai, T. Hirao, Synthesis of phosphonic acid ring-

substituted polyanilines via direct phosphonation to polymer main chains, RSC Adv. 7 (2017) 39306–39313. doi:10.1039/C7RA04678B.
View Article Online
DOI: 10.1039/D1TA10322A

[84] B. Martínez-Sánchez, D. Cazorla-Amorós, E. Morallón, Tailoring intrinsic properties of polyaniline by functionalization with phosphonic groups, Polymers. 12 (2020) 1–18. doi:10.3390/polym12122820.

[85] D.S. Yang, D. Bhattacharjya, S. Inamdar, J. Park, J.S. Yu, Phosphorus-doped ordered mesoporous carbons with different lengths as efficient metal-free electrocatalysts for oxygen reduction reaction in alkaline media, J. Am. Chem. Soc. 134 (2012) 16127–16130. doi:10.1021/ja306376s.

[86] F. Quesada-Plata, R. Ruiz-Rosas, E. Morallón, D. Cazorla-Amorós, Activated Carbons Prepared through H_3PO_4 -Assisted Hydrothermal Carbonisation from Biomass Wastes: Porous Texture and Electrochemical Performance, Chempluschem. 81 (2016) 1349–1359. doi:10.1002/cplu.201600412.

[87] L. Brožová, P. Holler, J. Kovářová, J. Stejskal, M. Trchová, The stability of polyaniline in strongly alkaline or acidic aqueous media, Polym. Degrad. Stab. 93 (2008) 592–600. doi:10.1016/j.polymdegradstab.2008.01.012.

[88] G. Socrates, Infrared and Raman characteristic group frequencies: Tables and charts., 3rd Ed., John Wiley & Sons, Chichester, UK, 2004.

[89] T. Jawhari, A. Roid, J. Casado, Raman spectroscopic characterization of some commercially available carbon black materials, Carbon. 33 (1995) 1561–1565. doi:10.1016/0008-6223(95)00117-V.

[90] E.F. Antunes, A.O. Lobo, E.J. Corat, V.J. Trava-Airoldi, A.A. Martin, C. Veríssimo, Comparative study of first- and second-order Raman spectra of MWCNT at visible and infrared laser excitation, Carbon. 44 (2006) 2202–2211. doi:10.1016/j.carbon.2006.03.003.

[91] S. Leyva-García, K. Nueangnoraj, D. Lozano-Castelló, H. Nishihara, T. Kyotani, E. Morallón, D. Cazorla-Amorós, Characterization of a zeolite-templated carbon by electrochemical quartz crystal microbalance and in situ Raman spectroscopy, Carbon. 89 (2015) 63–73. doi:10.1016/j.carbon.2015.03.016.